universität wien

MASTERARBEIT / MASTER'S THESIS

Titel der Masterarbeit / Title of the Master's Thesis

„Thermostatting in Ring Polymer Molecular Dynamics Simulations“

verfasst von / submitted by

Mag. Dr. Gerhard Tulzer BSc

angestrebter akademischer Grad / in partial fulfilment of the requirements for the degree of

Master of Science (MSc)

Wien, 2016 / Vienna, 2016

Studienkennzahl lt. Studienblatt / degree programme code as it appears on the student record sheet:	A 066 876
Studienrichtung lt. Studienblatt / degree programme as it appears on the student record sheet:	Masterstudium Physik
Betreut von / Supervisor:	a.o. Univ.-Prof. Dr. Martin Neumann

Acknowledgements

First and foremost, I would like to express my gratitude to a.o. Univ.-Prof. Dr. Martin Neumann, who not only introduced me to the field of computational physics and, in particular, the topic of quantum mechanical molecular dynamics simulations, but also advised this thesis project with great enthusiasm. Apart from being a chance to address the issues regarding this very thesis, the weekly meetings also included the discussion of topics of scientific work in general.

I am extremely grateful for the encouragement by my wife Michaela, who has always been there for motivating and also distracting me, each of course in the right moments. Her patience and understanding in the time of preparing this thesis can never be overestimated.

I would like to thank my whole family for their strong support during the whole period of academic studies. I am especially deeply grateful to my parents, who provided the possibility for an academic education in the first place.

Kurzfassung

In dieser Arbeit befassen wir uns mit der Implementierung von zwei Typen von Thermostaten in Ring-Polymer-Molekulardynamik-Simulationen.

Molekulardynamik-Simulationen sind bekanntermaßen ein wertvolles Hilfsmittel bei der Untersuchung von sowohl klassischen als auch quantenmechanischen molekularen Systemen. Bei letzteren ermöglicht die Verwendung des Pfadintegral-Formalismus die Auffassung von quantenmechanischen Teilchen als "beinahe-klassische" Ring-Polymere mit einem abgeänderten intermolekularen Potential.

Um ein thermisches Gleichgewicht herzustellen, also ein kanonisches Ensemble zu simulieren, werden Thermostate benötigt, welche die Interaktion des Systems mit einem Wärmebad imitieren. Natürlich gibt es hierfür viele verschiedene Typen, welche auf unterschiedlichen Ansätzen beruhen. Es stellt sich heraus, dass die Verwendung eines Gauß'schen Thermostats Resonanzen im Spektrum der Geschwindigkeits-Autokorrelationsfunktion hervorruft, was ein unerwünschter Effekt ist.

In dieser Arbeit konzentrieren wir uns auf den Ursprung der erwähnten Resonanzen sowie auf die Implementierung eines Langevin-Thermostats. Was ersteres Ziel betrifft, werden wir entdecken, dass die Resonanzfrequenzen den Eigenfrequenzen des Federsystems zwischen den einzelnen Monomeren entsprechen, auch wenn diese durch das intermolekulare Potential leicht verschoben sind.

Zweitens diskutieren wir die Implementierung eines Langevin-Thermostats, um die erwähnten Resonanzen zu beseitigen. Wir zeigen, dass das Spektrum in diesem Fall keine Resonanzen aufweist und untersuchen den Effekt der Kopplungsstärke zwischen System und Wärmebad. Außerdem vergleichen wir die Ergebnisse mit Daten einer *centroid molecular dynamics*-Simulation.

Abstract

This work deals with the implementation of two types of thermostats in ring polymer molecular dynamics (RPMD) simulations.

Molecular dynamics simulations have been proven to be a powerful tool in the investigation of molecular systems in the classical as well as in the quantum mechanical case. In the latter, the use of the celebrated path integral formalism allows to treat quantum mechanical particles as classical-like ring polymers with an alternative intermolecular potential.

In order to impose a thermal equilibrium condition, i.e. to simulate a canonical ensemble, a thermostat is needed, which mimics the interaction of a system with a heat bath. Of course, there exist many different types of thermostats with different approaches. It turns out that the use of a Gaussian thermostat leads to resonances in the velocity auto-correlation spectrum, which is an unwanted effect.

In this thesis, we focus on the investigation of the origin of the mentioned resonances and on the implementation of a Langevin thermostat. Regarding the first aim, it turns out that they correspond to the eigenfrequencies associated to the spring system of the ring monomers, although the intermolecular potential yields a slight shift of those frequencies.

Secondly, the implementation of a Langevin thermostat to overcome the mentioned issues is discussed in detail. We show that the spectrum is free of the resonances in this case and show the effect of the coupling strength to the heat bath. Additionally, we compare the results to data from simulations using the centroid molecular dynamics method.

Contents

Chapter 1

Introduction

Physical experiments dealing with molecular systems can suffer from non-negligible obstacles. Those range from extreme physical conditions like very low temperatures or very high pressures to situations where the quantity of interest, e.g. a thermodynamic quantity, is hardly accessible, which is often due to extremely low spatial and temporal scales. Theoretical studies, on the other hand, often lead to mathematical problems that cannot be treated analytically, such that a direct calculation is not possible. All the mentioned problems, both of experimental or theoretical nature, especially arise in statistical mechanics where many-body systems are investigated.

The establishment of computer simulations as a viable technique for the investigation of statistical mechanical systems has therefore become a tool of great importance in this area, since all the mentioned issues and hazards are irrelevant in this case. What matters here is mainly the requirement of a realistic microscopic interaction model, a stable numerical procedure, and appropriate techniques for the computation of the thermodynamic quantities of interest. For these reasons, computer simulations have become a main tool in the "experimental" investigation of classical as well as of quantum mechanical systems.

A widely used technique, especially for classical systems, is established by *molecular dynamics* simulations. The molecular dynamics method mimics physical motion by employing

interaction models between the system particles and calculating their motion according to the obtained intermolecular forces. The system is propagated in time using the associated Hamiltonian equations of motion. From the configuration as well as from the momenta of the particles, thermodynamic quantities can then be calculated, where needed relations are provided by statistical mechanics.

One of these quantities is the velocity auto-correlation function (VACF). This quantity is not only of interest for itself, but is also employed – together with the so-called *Gaussian approximation* [4, 60] – to calculate the self part of the intermediate scattering function. This quantity can be used further to, e.g. calculate the neutron cross section for H_2 [29] and D_2 [28]. The quantity we will be interested in the presented simulations is the spectrum of the velocity auto-correlation function.

Considering quantum mechanical systems, the situation is a little more complicated. However, a crucial breakthrough was made by Richard Feynman, who developed the celebrated *path integral* formalism, which allows to relate quantum mechanical monatomic systems to classical-like ring polymers, which can then be simulated employing the already established classical methods. This relation between quantum mechanical and ring-polymer systems has been termed *classical isomorphism*.

In order to impose a certain temperature to a system, so-called thermostats are used. Since the temperature regulation of a system is achieved via thermal contact to a heat bath which can be microscopically described in many different ways, there are also many different approaches to implement a thermostat for molecular dynamics simulations.

In this work, we will focus on two different types of those. We will see that the use of a Gaussian thermostat leads to resonances in the spectrum of the velocity auto-correlation function. Therefore, our goal will be to identify the source of those resonances, and present a different thermostat that does not show this effect. This will be the Langevin thermostat, which leads to a stochastic description of the heat bath coupling. The Langevin thermostat has already been employed in ring polymer molecular dynamics simulations (e.g. [17]), but not yet for the investigation of the velocity auto-correlation function and its spectrum.

We will focus on ortho-deuterium as a model system throughout this thesis, since it is very well-studied and provides a very simple structure, which prevents losing ourselves in computational and implementational details.

This thesis is organized as follows. In Chapter 2, we are going to summarize the necessary concepts of statistical mechanics, both for the classical and the quantum mechanical case. We discuss the concept of ensembles as well as the approach for theoretically calculating thermodynamic quantities.

Chapter 3 is devoted to an introduction to molecular dynamics simulations, which constitute the basis for the simulations performed in this thesis.

We present the path integral formalism in Chapter 4, and also briefly discuss the path integral Monte Carlo method.

Chapter 5 addresses the extension of the path integral formalism for quantum molecular dynamics simulations, where the Boltzmann factor needs to be extended such that dynamical information is introduced to the system. We then describe several particular techniques for the simulation, including basic path integral molecular dynamics, centroid molecular dynamics (CMD), and ring polymer dynamics (RPMD) simulations.

The explicit methods as well as details of the implementation, including the used algorithm, which is based on the discussion in [17], are presented in Chapter 6.

With all those preparations, we are ready to present our results in Chapter 7, where we discuss the issues arising in RPMD simulations employing the isokinetic ensemble, and identify the source of the arising resonances. We compare those results to data from simulations employing the Langevin thermostat, and show the dependence on different coupling strengths. Those results are in turn compared to data obtained from CMD simulations.

Chapter 8 summarizes our achievements.

Chapter 2

Some Statistical Mechanics

The laws of thermodynamics have been derived based on a phenomenological investigation of macroscopic systems. From these, a great number of physical results have been derived, which have not only been important for scientific reasons, but also led to very useful applications in daily life. However, all these findings do not predict any microscopic behavior of the physical system. Relating the results of thermodynamics to microscopical effects is not at all trivial. As a consequence, there is a whole theory which aims at finding relations between these two levels of interest: *statistical mechanics*. As large and important this area is, we will not present a detailed introduction, but rather discuss the main concepts relevant for this thesis in the following sections.

We will start this chapter with a discussion of two important concepts in statistical mechanics, which are the *microcanonical* and the *canonical ensemble*. We will define them and explain how static macroscopic quantities are derived from the microscopic behavior in such systems. We then describe the canonical ensemble for quantum mechanical systems in Section 2.3. Since we are also interested in dynamic quantities which relate observables at certain time differences, we introduce and discuss correlation functions for classical as well as for quantum mechanical systems in Section 2.4. Finally, in Section 2.5, we present a first glimpse on the numerical methods to compute the high-dimensional integrals defining thermodynamic quantities.

2.1 The Microcanonical Ensemble

Consider a system of N particles in a volume V in thermodynamic equilibrium. If we know all the positions and all the velocities of these particles at a given time, we can, under the assumption that the particles behave as classical mechanics tells us, use the equations of motion to calculate the state of the system at any time we want. Let us consider the $6N$-dimensional space consisting of $3N$ position coordinates and $3N$ momentum coordinates, where each set of positions and momenta of the system represents a point in this so-called *phase space*. The evolution of the system state in time will then create a path in the phase space, and it will turn out that there are certain restrictions as to which points can be reached by a specific system. As an example, consider the system to be closed, i.e. no energy is transferred to or from the system. Then, the possible states of the system form a hyperplane in the phase space, comprising all points that correspond to a fixed value for the Hamiltonian of the system, which is of course equal to the total system energy.

Since we have fixed certain quantities (N, V, and E, in this case), each state in the corresponding phase space describes a closed macroscopic system with those parameters. However, there are many more parameters that can be assigned to a macroscopic system, including pressure or temperature, or more complicated ones like mean distances between particles. While the quantities of the first category can be manipulated (in the sense of prescribing them), the ones from the second category cannot, as they will depend on the prescribed ones (and, of course, on the microscopic configuration). The question now is: Can their values be determined anyway, and if yes, how can this be achieved? What is the pressure, or the temperature, of the macroscopic system if it is different for each microscopic one? The basis for the solution is provided by the main assumption of statistical mechanics, which is the *postulate of equal a-priori probability.*

Postulate (Equal a priori probability)
For an isolated system in equilibrium, all microscopic states consistent with the given macroscopic quantitites are taken by the system with equal probability.

Using this postulate, the way to find out the quantities of interest is straightforward. Roughly speaking, we just need to have the system in a representative collection of microscopic states, log the respective quantity each time, and finally calculate the average. Note that this is also the method of choice for typical physical measurements, where usually, the outcome is never exactly the same, but will fluctuate a bit. Therefore, we perform experiments several times in order to calculate error bounds for the measured quantities.

The set of microscopic states is a very important concept, such that it is advantageous to give it a specific name. A collection of systems comprising all the possible microscopic states

consistent with given macroscopic parameters is therefore called *ensemble*. As an example, the ensemble for systems with fixed particle number, volume and total energy is called *microcanonical ensemble*, and will be discussed in the following paragraphs.

In order to be able to perform calculations based on ensembles, we first need to know the number of microscopic states consistent with the macroscopic parameters. This quantity is called *partition function*, or sometimes *sum over states*. It is basically derived by counting the states in the subset of the phase space, which, for the microcanonical ensemble leads to

$$\Omega(N,V,E) = \frac{1}{N!h^{3N}} \int\limits_{E<\mathcal{H}(\mathbf{p},\mathbf{q})<E+E_0} \mathrm{d}^{3N}\mathbf{p}\,\mathrm{d}^{3N}\mathbf{q} \approx \frac{E_0}{N!h^{3N}} \int \mathrm{d}^{3N}\mathbf{p}\,\mathrm{d}^{3N}\mathbf{q}\,\delta\left[\mathcal{H}(\mathbf{p},\mathbf{q}) - E\right], \tag{2.1}$$

where $E_0 \ll E$, such that the integral is over a very thin shell above the constant-energy hypersurface. Here, h denotes the Planck constant, which has been introduced to make Q dimensionless, and $\mathcal{H}(\mathbf{p},\mathbf{q})$ is the Hamiltonian of the system. The factor $(N!)^{-1}$ is added to account for the correct Boltzmann counting. Note that, while we integrated over the energy shell in the first integral, we are integrating over the whole phase space in the second one by using a Delta-function.

As we said, the partition function gives us the number of accessible microscopic states under the prescribed thermodynamic conditions. Remembering the postulate of equal a priori probability, we can also derive a probability distribution for the microscopic states. It is given by

$$P = \begin{cases} \frac{1}{\Omega(N,V,E)} & \text{if } E < \mathcal{H} < E + E_0 \\ 0 & \text{else,} \end{cases} \tag{2.2}$$

which, in the limit $E_0 \to 0$, can be rewritten as

$$P = \frac{1}{\Omega(N,V,E)}\delta\left[\mathcal{H} - E\right]. \tag{2.3}$$

Note that with this definition the partition function acts as a normalizing constant. Then, if we want to calculate the value of an observable $\mathcal{A}(\mathbf{p},\mathbf{q})$ depending on $\mathbf{p}$ and $\mathbf{q}$, we can do this via

$$A = \langle\mathcal{A}\rangle = \frac{E_0}{N!h^{3N}\Omega(N,V,E)} \int \mathrm{d}^{3N}\mathbf{p}\,\mathrm{d}^{3N}\mathbf{q}\,\mathcal{A}(\mathbf{p},\mathbf{q})\,\delta\left[\mathcal{H}(\mathbf{p},\mathbf{q}) - E\right], \tag{2.4}$$

which is the standard definition of an expected value with the probability distribution defined in equation (2.3).

2.2 The Canonical Ensemble

The microcanonical ensemble proves to be a very convenient theoretical starting point. However, the fact that it is very complicated or even impossible to obtain closed systems in experiments makes the use of the microcanonical ensemble unfavorable. Rather, because experimentally easier achievable, we should have an ensemble with fixed temperature instead of total energy. This results in the consideration of the *canonical ensemble*, which will also be used throughout this thesis. To obtain it, consider a physical system in contact with a heat bath, such that this combined system is closed, hence may be treated as a microcanonical ensemble. Then the physical sub-system we are interested in will exhibit the properties of a canonical ensemble.

Due to the thermal contact between the physical system and its heat bath, which leads to different possible energies for the physical system, the postulate of equal a priori probability is not valid any more, such that the probabilities for given microscropic states are not uniformly distributed. In fact, for a microscopic state with energy E, the probability for the physical system to be in this state $P(E)$ is now proportional to

$$P(E) \propto \mathrm{e}^{-\beta E}, \tag{2.5}$$

where $\beta = (k_B T)^{-1}$. With this, the partition function for the canonical ensemble is given by

$$Q(N,V,T) = \frac{1}{N! h^{3N}} \int \mathrm{d}^{3N}\mathbf{p}\, \mathrm{d}^{3N}\mathbf{q}\, \mathrm{e}^{-\beta \mathcal{H}(\mathbf{p},\mathbf{q})}. \tag{2.6}$$

This means that in the canonical ensemble the probabilities of the microscopic states are weighted by a factor depending on the sub-system's total energy. This factor, is called *Boltzmann factor*. The expected value for an observable is therefore

$$A = \langle \mathcal{A} \rangle = \frac{1}{N! h^{3N} Q(N,V,T)} \int \mathrm{d}^{3N}\mathbf{p}\, \mathrm{d}^{3N}\mathbf{q}\, \mathcal{A}(\mathbf{p},\mathbf{q})\, \mathrm{e}^{-\beta \mathcal{H}(\mathbf{p},\mathbf{q})}. \tag{2.7}$$

Remark

There are other ensembles that also appear to be suitable for comparison with experimental data, such as the isothermal-isobaric ensemble, where N, the pressure p, and T are fixed, or the grand canonical ensemble, where the chemical potential μ, V, and T are prescribed. It can even be shown that these two ensembles are very similar to the canonical ensemble in the sense that the corresponding results for simple observables are not too far apart, and that the conversion is very simple in the thermodynamical limit [70].

2.3 The Canonical Ensemble in Quantum Mechanics

So far, we have discussed classical ensembles. Of course, the notion of an ensemble can be generalized to the quantum mechanical case. In fact, the classical canonical partition function given in equation (2.6) is then the classical limit for the quantum mechanical partition function. We will now have a closer look at the generalized formulation of this very ensemble.

For a quantum mechanical system in a mixed state $|\Psi\rangle$, there exist orthogonal pure states $|\Psi_n\rangle$ which comprise the possible states the system can assume in case of a measurement. If each of these states is assumed with probability p_n, the *density operator* is given by

$$\hat{\rho} = \sum_n p_n \left|\Psi_n\right\rangle \left\langle\Psi_n\right| . \tag{2.8}$$

The corresponding *density matrix* is then

$$\rho_{kl} = \left\langle\Psi_k|\hat{\rho}|\Psi_l\right\rangle . \tag{2.9}$$

We now use the density matrix for considering the expected value of an observable A. While for pure states the result is pretty simple, where we obtain $\left\langle\hat{A}\right\rangle_n = \langle\Psi_n|\hat{A}|\Psi_n\rangle$, for mixed states we have to take into account all possible pure states. This leads to

$$\langle A\rangle = \sum_n p_n \langle\Psi_n|A|\Psi_n\rangle = \sum_n \rho_{nn} A = \mathrm{Tr}\left[\rho A\right] . \tag{2.10}$$

For a quantum mechanical ensemble, the density matrix is therefore a measure for the probability that each microstate compatible with the macroscopic prescriptions is attained, and is therefore the quantum mechanical correspondence of the phase space distribution. In particular, for the canonical ensemble, where we fix the particle number N, the volume V and the temperature T, we have

$$\hat{\rho} = \frac{\mathrm{e}^{-\beta\hat{\mathcal{H}}}}{Q(N,V,T)}, \tag{2.11}$$

where the related partition function is

$$Q(N,V,T) = \mathrm{Tr}\left[\mathrm{e}^{-\beta\hat{\mathcal{H}}}\right] . \tag{2.12}$$

The expected value for an observable $\hat{A}$ can therefore be written as

$$\left\langle\hat{A}\right\rangle := \frac{\mathrm{Tr}\left[\hat{A}\mathrm{e}^{-\beta\hat{\mathcal{H}}}\right]}{Q(N,V,T)} = \frac{\mathrm{Tr}\left[\hat{A}\mathrm{e}^{-\beta\hat{\mathcal{H}}}\right]}{\mathrm{Tr}\left[\mathrm{e}^{-\beta\hat{\mathcal{H}}}\right]} \tag{2.13}$$

2.4 Dynamical Properties

In the previous sections, we have described how to handle different ensembles and defined averages for certain observables. These observables all corresponded to time-independent, or *static*, properties. Examples for those are internal energy, the radial distribution function, or the net electric dipole moment in a polar liquid. It turns out that there are several methods to assess these quantities for classical as well as for quantum-mechanical systems (see [2, 27, 70]).

However, there are a lot of very interesting quantities that depend on time – or rather on time differences. The most important ones of this type are diffusion constants, chemical reaction rates, or thermal conductivities. Since these *dynamical* quantities have, by definition, their origin in non-equilibrium systems, their calculation is not directly possible. Luckily, *linear response theory* allows to relate their values to correlation functions of the system.

Let us us start with the classical case. Given two observables A and B for a classical system the corresponding correlation function is given by

$$C_{AB}(t) = \langle A(0)B(t)\rangle = \frac{1}{Q}\int \mathrm{d}^{3N}\mathbf{p}\mathrm{d}^{3N}\mathbf{q}\,\mathrm{e}^{-\beta\mathcal{H}(\mathbf{p},\mathbf{q})}A(0)B(t). \tag{2.14}$$

Since only the time difference matters, we can always consider one observable at $t = 0$.

It is not only interesting to study the correlation between to different observables. Rather, one is often interested in the correlation of a quantity with itself. The straightforward definition of the *auto-correlation function* is then

$$C_{AA}(t) = \frac{1}{Q}\int \mathrm{d}^{3N}\mathbf{p}\mathrm{d}^{3N}\mathbf{q}\,\mathrm{e}^{-\beta\mathcal{H}(\mathbf{p},\mathbf{q})}A(0)A(t). \tag{2.15}$$

Obviously, both of these definitions are, like the definitions of expected values, phase-space integrals which we can consider as an expected value for an observable product.

Turning to quantum mechanical systems now, we quickly encounter a problem. Since operators in quantum mechanics do not commute in general, there are different possibilities to define correlation functions.

The "standard" definition for a quantum mechanical correlation function is, analogeously to the classical case, written as the expected value for an operator product,

$$C^{QM}_{AB}(t) := \frac{1}{Q}\,\mathrm{Tr}\left[\mathrm{e}^{-\beta\hat{\mathcal{H}}}\hat{A}(0)\hat{B}(t)\right] = \frac{1}{Q}\,\mathrm{Tr}\left[\mathrm{e}^{-\beta\hat{\mathcal{H}}}\hat{A}\mathrm{e}^{i\hat{\mathcal{H}}t/\hbar}\hat{B}\mathrm{e}^{-i\hat{\mathcal{H}}t/\hbar}\right], \tag{2.16}$$

where the exponential with the complex exponent is the time evolution operator in the Heisenberg picture. A drawback of this definitions is the missing symmetry. As an example, for

hermitian position-dependent operators, the correlation function is complex, while the classical autocorrelation function is real and even.

Another possibility to define the correlation function is the so-called *Kubo-transformed* correlation function [40], which is written as

$$C_{AB}^{K}(t) := \frac{1}{\beta Q} \int_0^\beta \mathrm{Tr}\left[\mathrm{e}^{-(\beta-\lambda)\hat{\mathcal{H}}} \hat{A}(0) \mathrm{e}^{-\lambda\hat{\mathcal{H}}} \hat{B}(t)\right]. \tag{2.17}$$

Although this definition is different to equation (2.16), there is a simple relation between their Fourier transforms,

$$C_{AB}^{QM}(\omega) = \frac{\beta\hbar\omega}{1-\mathrm{e}^{-\beta\hbar\omega}} C_{AB}^{K}(\omega), \tag{2.18}$$

which allows to easily go back and forth between these two. Here, the Fourier transform is given by

$$C_{AB}(\omega) = \frac{1}{2\pi} \int_{-\infty}^{\infty} \mathrm{d}t\, \mathrm{e}^{-i\omega t} C_{AB}(t) \tag{2.19}$$

The big advantage of the Kubo-transformed correlation function is its higher symmetry. As an example, for hermitian position-dependent operators, the correlation function is real and even like in the classical case [21].

The main drawbacks from the computational side is that correlation functions can, for general quantum mechanical systems, only be approximated. To perform this task, several methods have been developed, but up to now, no method of choice exists, since each one has its disadvantages. These different methods will be discussed in more detail in Chapter 5.

2.5 Sampling and Averaging in Practice

Having derived expressions for thermodynamic quantities, we are facing the integration of integrals over spaces with $6N$ dimensions, where, for a macroscopic system, $N \approx 10^{23}$. Furthermore, no analytic expressions for the solutions exist in general. The explicit calculation of such integrals is therefore way out of reach. However, methods have been developed to numerically calculate those integrals for very small systems with up to several thousand particles. Of course, these calculations cannot be performed by hand, but involve the use of computers. Over time, there have been two main approaches which each have their advantages and drawbacks. These are *Monte Carlo* simulations and *Molecular Dynamics* simulations.

Monte Carlo simulations are stochastic methods to approximate integrals relying on the *central-limit theorem*. They go back to the work of Enrico Fermi, and were later heavily used in the *Manhattan Project*. Basically, this technique has been developed to approximate high-dimensional integrals, for which it is still used in many disciplines. For the use in statistical mechanics, the method is based on the random generation of accessible microscopic states and subsequent calculation of the mean value over the quantity measured in each of those states. A very effective approach is based on the fact that in equation (2.7) we have a ratio of two integrals. Metropolis [47] developed a method that very efficiently samples expressions of this type, which has become the standard method for Monte Carlo simulations in statistical mechanics. For further information on this method, see [2, 27, 70].

2.6 Conclusions

As might have become clear from the few introductory words on this technique, the Monte Carlo method is perfectly suitable for the calculation of static properties of a microscopic system. However, in its basic version, it does not contain any dynamical information on the particles whatsoever. Although this makes it appropriate for simulations of systems that cannot be related to dynamical features (e.g. the Ising model), this is a huge drawback if we are interested in dynamical information. Therefore, we will now turn to a method that naturally describes particle motion.

Actually, this method is even fundamentally based on the microscopic dynamics of the system under investigation. Here, rather than sampling over different systems we only consider one of them. Then, in order to obtain the expected values of interest, either for simple observables or for correlation functions, we rely on the *ergodic hypothesis*.

Hypothesis (Ergodic Hypothesis)
A dynamical system is called ergodic if given any allowed initial condition each microscopic state consistent with the thermodynamic parameters is visited with non-zero probability.

This property of ergodic systems allows to identify the mean over the ensemble with the mean over a single system evolving over time,

$$A = \frac{1}{N!h^{3N}Q(N,V,T)} \int \mathrm{d}^{3N}\mathbf{p}\,\mathrm{d}^{3N}\mathbf{q}\,\mathcal{A}(\mathbf{p},\mathbf{q})\,\mathrm{e}^{-\beta\mathcal{H}(\mathbf{p},\mathbf{q})} = \frac{1}{T}\int_0^T \mathrm{d}t\,A(\mathbf{p}(t),\mathbf{q}(t)). \quad (2.20)$$

Thus, we can use the equations of motion to evolve the system and calculate the desired quantities after each performed timestep, thereby also yielding a sufficient number of samples

to calculate the averages. This method is called *Molecular Dynamics*. Research on the method itself as well as using it has become huge, which is mainly due to its versatility. Since it is also used in this work, we refer to the following chapter for detailed explanations.

Chapter 3

Molecular Dynamics Simulations

The method of molecular dynamics simulations for classical mechanics is a straightforward approach to investigate macroscopic quantities of a system by considering its microscopic behavior. In particular, it allows the calculation of static as well as dynamic properties of the system. Computer simulations are very similar to physical experiments or can even be thought of as *virtual* experiments. They enable the testing of hypotheses and generate information about the investigated system, where their great advantage is the versatility of the system. As an example, simulations at very high pressures or low temperatures are not more difficult to perform than at pressures or temperatures arising naturally, while a physical experiment under the same conditions might not only be a considerable challenge, but also affected by severe safety issues. The main drawback, however, is the need of a properly working model in order to be able to mimic the physical processes taking place. For many systems, this challenge has been accomplished, which makes computer simulations a widely used tool in the scientific community.

We start the chapter by a short review of the history of computer simulations. Then, we will explain the derivation of the molecular dynamics method for the classical case, present the chosen algorithm for the numerical integration in more detail, where we also include thermostatting approaches. This description is mainly based on the books by Allen & Tildesley [2], Frenkel & Smit [27] and Tuckerman [70].

3.1 Some History of Computer Simulations

The driving force for the development of computer simulations was the desire to test theories concerning dense liquids. For a long time, there was almost no way to obtain any verification for theoretical approaches, where the best that could be done were mechanical models developed by Bernal [5]. The first approach using computers was developed in Los Alamos in 1953, where Metropolis and his co-workers developed the now famous *Monte Carlo* technique to model a two-dimensional fluid [47]. The next step was the integration of the equations of motion for a one-dimensional anharmonic chain, performed by Fermi, Pasta and Ulam [25]. Simulating the movement of hard spheres in 1956 by Alder and Wainwright [1] can be considered the first molecular dynamics simulation, while the first simulation using realistic continuous potentials of a liquid was performed in 1964 by Rahman for argon atoms [59]. Soon, more sophisticated structures starting from diatomic molecules [33] to liquid water [61] to much more complicated molecules like proteins [42, 46] could be simulated. The range of possible applications increased when Andersen introduced a molecular dynamics method for NVT and NPT ensembles [3], which allowed direct comparison to the more easily performable physical experiments at constant temperature or pressure.

Another milestone was the extension of computer simulation methods to quantum mechanical systems. One of the groundbreaking steps here was the introduction of the computationally expensive, so-called *ab-initio* simulations by Car and Parrinello [14], where the electronic structure is directly used to calculate the interactions between the molecules.

Based on the much earlier works on quantum mechanical systems by Richard Feynman [26], two approaches have evolved for simulations using the path integral formalism. On the one hand, the first *path integral Monte Carlo* (PIMC) simulations have been performed by Ceperley & Pollock [16]. This method allows the exact calculation of static properties of the system. On the other hand, several methods based on molecular dynamics have been developed, ranging from basic *path integral molecular dynamics* (first performed by Parrinello and Rahman [55] as well as by Hall and Berne [32]) to *centroid molecular dynamics* (first performed by Cao & Voth [10, 11, 12, 13]) and *ring polymer molecular dynamics* simulations (first publishe by Craig and Manolopoulos [20, 21]). Although the latter category only allows an *approximate* calculation of dynamical quantities, they show very good results under certain conditions. A more detailed description of these methods will be provided in Chapters 4 and 5.

The first path integral molecular dynamics simulations have been performed by Parrinello and Rahman [55] as well as by Hall and Berne [32]. Since then, many different refinements and adaptations have been developed. This includes especially *centroid molecular dynamics* [10, 11, 12, 13] as well as *ring polymer molecular dynamics* [20, 21] simulations. Since the latter one is the method of choice in this work, we will go into further detail later on.

3.2 The Molecular Dynamics Technique in a Nutshell

The idea of molecular dynamics simulations is to follow the trajectories of all the particles in a system and calculate specified quantities of interest at every other time throughout the simulation. The calculation of the trajectories boils down to solving the classical N-body problem. Evaluating the statistics of the sampled quantities yields then numerical values for thermodynamical as well as for structural parameters of the investigated system. This is possible since all these quantitites can be related not only to the positions and the velocities of the particles at given times, but to their time correlation functions and their spectra as well. These relationships will be discussed later in this thesis.

The fundamental basis for this technique are Newton's equations of motion, the solution of which gives the trajectories of each particle belonging to the system. Analytic solutions to Newton's equations of motion can only be found for cases involving only up to two particles or for certain, e.g. harmonic, potentials. However, when considering realistic systems, which usually involves many particles and complicated potentials, there is only a numerical solution attainable. To perform the necessary calculations, powerful algorithms are needed in order to obtain suitable results within proper timespans. Many different types of algorithms, such as *Verlet* algorithms, *symplectic* methods, or *predictor-corrector* methods have been developed.

Performing a molecular dynamics simulations boils down to the following steps:

(i)	initialization,
(ii)	equilibration,
(iii)	measurement,
(iv)	evaluation of the data.

The initialization step consists of assigning starting positions and velocities for all system particles which are compatible with the constraints applied to the system. This task is fairly simple, although there are some pitfalls that must to be avoided. In particular, a poor initialization might lead to blow-ups of the numerical solution due to extremely large numbers arising in the first steps of the time evolution. These might occur, e.g., when two particles are very close together or even overlap and the resulting forces are huge.

A very simple approach to avoid this trap, which is also followed in the simulations conducted for this work, is to put the particles on a lattice, which naturally avoids overlapping. Usually, the lattice type which is naturally assumed by the respective crystallized system is employed for this task. For spherical particles, this is the face-centered cubic configuration, which allows

the highest densities without overlapping. The lattice constants need to be chosen according to the prescribed density. By choosing suitable density and temperature for a liquid system, the initialized crystal should then melt within a reasonable time.

The initialization of the velocities, on the other hand, is very straightforward. In particular, one can assign values drawn from a uniform distribution. After that, one only needs to shift the values such that the total momentum vanishes, and to rescale the values according to the prescribed constraint like a given kinetic energy.

After the initialization, the system will in general not be in equilibrium. If we started to record data right from the beginning, we would also measure quantities that belong to another state of the system and therefore distort our results. As a consequence, we let the system evolve for some time until it has reached equilibrium. Then, we are ready to log information.

The actual logging phase of the simulation is, of course, the most time consuming step. It consists mainly of three steps that are repeated very many times in order to obtain proper mean values. These steps are the calculation of the forces, the propagation of particle positions and velocities, and the calculation of the quantities of interested in the current configuration. All these steps will be explained in further detail below.

After a simulation is finished, we need to make sense of the data we recorded. This might on the one hand just be the averaging over a sampled quantity, or on the other hand require the calculation of a correlation function or a corresponding spectrum. Examples of this will be given below, when we discuss the post-processing of the simulation.

A sketch of the course of a simulation (where we show the average potential energy sampled from the beginning of the simulation) is shown in Figure 3.1.

3.3 Small Systems

The simulation of a physical system becomes very complex with increasing number of molecules. Therefore, one is usually limited to the consideration of systems with up to $\mathcal{O}(10^8)$ particles in simple systems. Compared to a typical system size (1 mol $\approx 10^{23}$ molecules), this number is extremely low. The main problem with this is the influence of surface effects. These arise since the particles at the surface are not surrounded by other system particles and therefore will encounter different interactions than their bulk counterparts. A simple estimation of the number of surface particles in a system shall underline this problem.

Consider a simple lattice consisting of 1000 particles, yielding a $10 \times 10 \times 10$ lattice. There, the surface of the lattice is formed by 488 particles, which is almost half of the molecules. On

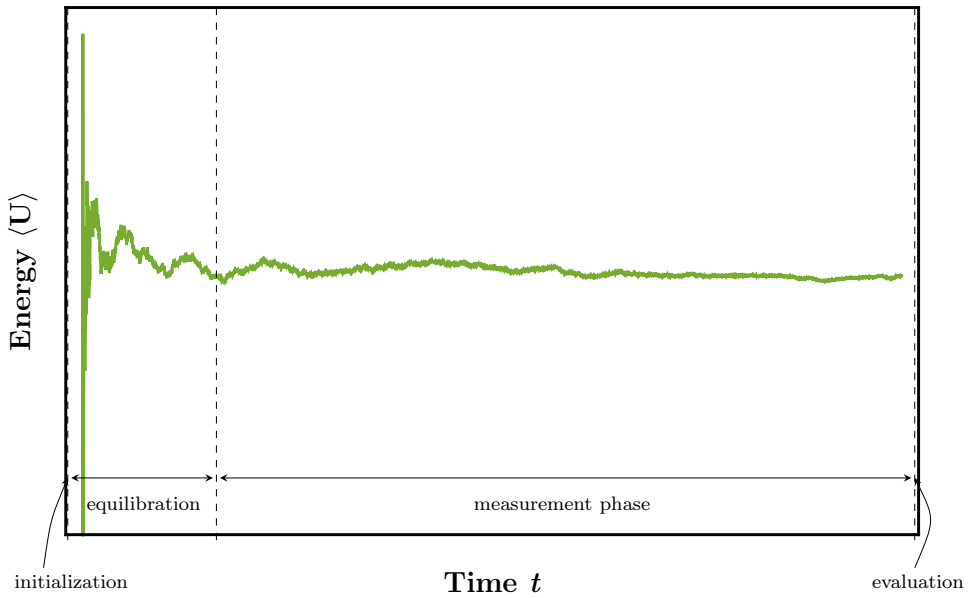

Figure 3.1: A sketch of the typical course of a simulation. After the initialization, some time is needed to equilibrate the system. Most of the time is then needed for the sampling of the quantities of interest. At the end of the simulation, the obtained data is evaluated in a post-processing step.

the other hand, considering a lattice made of $10^8 \times 10^8 \times 10^8 = 10^{24}$ particles, we have approximately 6×10^{16} surface particles, which is about $6 \times 10^{-8}\%$. It is clear that in macroscopic systems, surface effects can be neglected, while some work-around is needed in the simulated system.

The solution in this case is the implementation of periodic boundary conditions, which belongs to the standard techniques in molecular dynamics simulations. Their use has been first presented in [7]. This means that we identify opposite boundaries of our simulation domain. One can think of this as periodically extending the simulation domain in all directions, where all copies of the original particle move in the exact same way. Therefore, if a particle leaves the original domain, one of its copies will enter the domain on the opposite side. A two-dimensional sketch of this situation is shown in Figure 3.2.

Note that a natural bound for long-range phenomena or long-wavelength fluctuations is the size of the simulation domain. Therefore, if such effects are to be studied, it is necessary to increase the size of the box and, accordingly, the system.

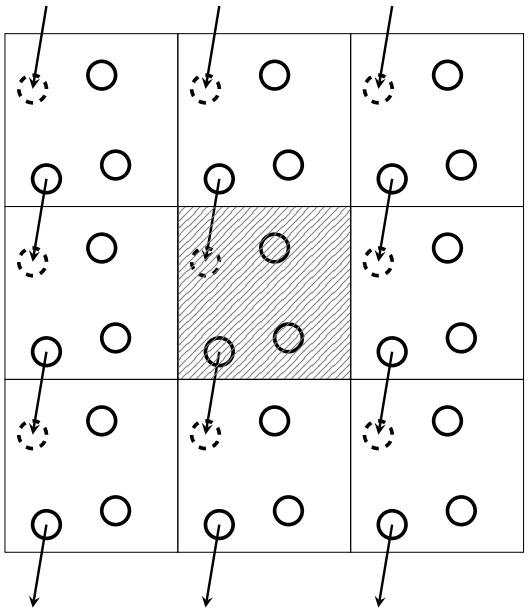

Figure 3.2: Two-dimensional sketch of the periodically extended simulation domain. The hatched box is the original domain. If one particle leaves it, one of its periodical counterparts enters the box across the opposite boundary. Figure based on [2].

3.4 Integration Algorithms – Force Calculation

The integration of Newton's equations of motion mainly involves two parts. On the one hand, there is the calculation of the forces acting on each of the particles. This step is very time-consuming and needs special attention such that we can save some computational cost. On the other hand, there is the evolution of the positions and the momenta. Although extreme accuracy of the trajectories is not necessary to a proper evaluation of the macroscopic quantities, the most important topic here is a certain degree of stability of the algorithm.

The method of calculating the acting forces is of the utmost importance, since two factors play a significant role. First, a suitable interaction model needs to be chosen in order to obtain results that can be matched with real-world experiments. Second, if the force calculation is done naively, a lot of computation time will be wasted.

The interactions between the system particles are defined via a potential $\mathcal{U}$ that influences the movement of every particle, depending on the location of all the other particles. The most simple ansatz for this potential is obtained by only considering pair interactions. In

many cases, especially for simple molecules, this approach gives quite good results, and is therefore widely used. In this case, the potential depends only on the distance between the two particles. The resulting forces acting on the molecules are then obtained via

$$F_i = -\frac{\partial \mathcal{U}(\boldsymbol{r})}{\partial r_i}, \tag{3.1}$$

where F_i is the force on particle i. Note that the potential depends on all the particle coordinates, which is indicated by the bold notation.

A well studied and widely used pair potential is the *Lennard-Jones* potential, which combines simplicity and accuracy for many different, but especially spherical substances for proper choices of the included parameters. This type of potential is particularly suitable for inert gases like Ar, Xe, or Kr, and is given by

$$\mathcal{U}(r) = 4\varepsilon \left[\left(\frac{\sigma}{r}\right)^{12} - \left(\frac{\sigma}{r}\right)^{6} \right]. \tag{3.2}$$

This choice yields a potential with a well of depth ε, and an assumed particle diameter of σ, where the numerical values for ε and σ depend on the investigated substance. The shape of the Lennard-Jones potential is shown in Figure 3.3.

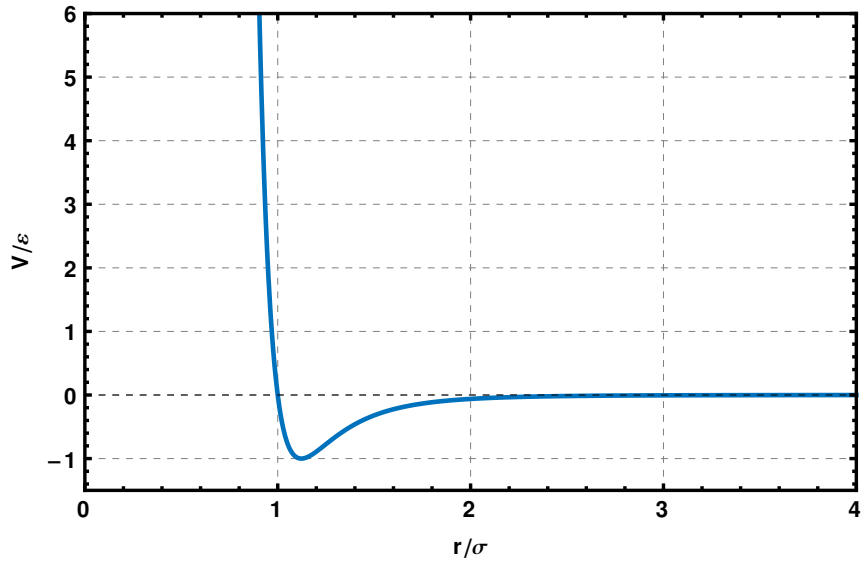

Figure 3.3: The shape of the Lennard-Jones potential. For distances lower than $2^{1/6}\sigma$, the potential is repulsive. The potential depth is given by ε.

It is obvious that the force is repelling for distances smaller than $r_m = 2^{1/6}\sigma$. Furthermore, it is notable that for distances larger than 3σ, the potential is approximately zero, which underlines the short-range character of the potential. Note that there are many other types of potentials (so-called *realistic* potentials) that model certain aspects of a specific system more accurately than the Lennard-Jones potential. An example is the *Silvera-Goldman* potential [65] for H_2 and D_2, which will be used later on in this work.

However, even for these most simple pair interaction models, the computational cost might become enormous for systems with typical numbers of particles, since after the implementation of periodic boundary conditions, in theory each molecule interacts not only with the molecules in the original box, but also with all their periodic images, which are, in theory, infinitely many. Since for n particles the number of interactions is $\mathcal{O}(n^2)$, it is absolutely necessary to come up with some trick to lower the number of force evaluations. The solution is pretty straightforward and has become a standard technique.

We remember that a short-ranged potential is approximately zero after a few multiples of the particle diameter (see the Lennard-Jones potential in Figure 3.3). Therefore, as a first step, we apply the *minimum image convention*. This means that for a fixed molecule we only take into account interactions with the particular image of each other particle which is closest to the fixed molecule. In the second step, the actual force calculation, we will then consider the interaction between two particles negligible if their distance is larger than a certain *cut-off distance*. Since many particles will be beyond the cut-off distance, we can again save a lot of work through this approach. As an example, in a 3D simulation box, we can disregard almost half of all the particle interactions, even if we choose the maximum possible cut-off ($r_c = L/2$). The concept of the minimum image convention together with a potential cut-off distance is shown in Figure 3.4.

Despite the usefulness of pair interaction models, it turns out that certain macroscopic quantities obtained in experiments cannot be predicted correctly without considering many-body interactions [23, 61]. This is especially the case for crystals. The best strategy to follow here is to slightly adapt the exact pair interactions to obtain *effective* pair interactions. There exist several approaches depending on the system of consideration, including the embedded atom method [24] or the *Stillinger-Weber* potential [66], which even includes direction-dependent terms. This is mostly necessary for non-spherical particles. It is obvious that more complicated potentials require more computational power and memory.

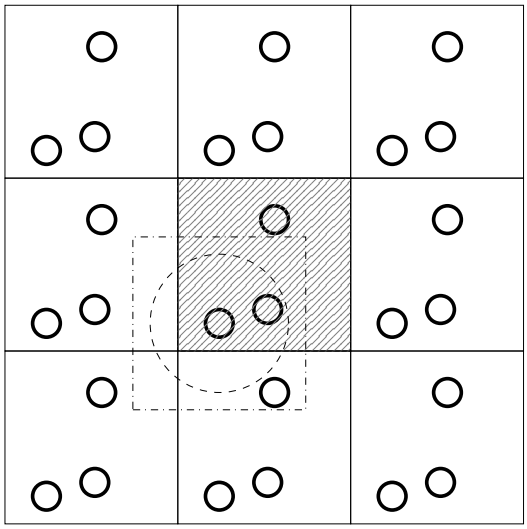

Figure 3.4: Two-dimensional sketch illustrating the minimum image convention. All particles within the dash-dotted square are the nearest neighbours to the particle in the center of this box, and are therefore considered for interaction. Using the dashed circle as a cut-off radius, we would only calculate the interaction with one other molecule, while the third particle is too far away. Figure based on [2].

3.5 Time Evolution

The time evolution of the system is given by the Hamiltonian equations of motion, which read

$$\dot{p_i} = -\frac{\partial \mathcal{H}}{\partial q_i} \qquad \dot{q_i} = \frac{\partial \mathcal{H}}{\partial p_i}, \tag{3.3}$$

where $\mathcal{H}$ is the Hamiltonian of the system and p_i and q_i denote the momentum and the position of the i-th particle, respectively For a classical system, the Hamiltonian is given by

$$\mathcal{H}(\mathbf{p}, \mathbf{q}) = \sum_{i=1}^{N} \frac{p_i^2}{2m_i} + \mathcal{U}(\mathbf{q}), \tag{3.4}$$

where m_i denotes the particle mass and $\mathcal{U}_i$ denotes the potential that the i-th particle feels.

We have already mentioned that there are many different approaches to integrate the equations of motion. Here, we will explain the *velocity Verlet* algorithm [67] in detail, since it shows several favorable properties. It is an extension of the previously developed *Verlet* algorithm [72] which evolves both positions and momenta explicitly, and is based on an Taylor series

expansion of the position of particle i at a time $t + \Delta t$,

$$\begin{aligned}\mathbf{r}_i(t+\Delta t) &= \mathbf{r}_i(t) + \Delta t\dot{\mathbf{r}}_i(t) + \frac{\Delta t^2}{2}\ddot{\mathbf{r}}_i(t) + \mathcal{O}(\Delta t^3) \\ &= \mathbf{r}_i(t) + \Delta t\mathbf{v}_i(t) + \frac{\Delta t^2}{2m_i}\mathbf{F}_i(t) + \mathcal{O}(\Delta t^3),\end{aligned} \tag{3.5}$$

where we have used Newton's second law to replace the second derivative by the force. Here, $\mathbf{r}_i(t)$ and $\mathbf{v}_i(t)$ denote the location and the velocity of particle i, respectively, while $\mathbf{F}_i(t)$ denotes the force acting on it at this time. Conversely, we can express $\mathbf{r}_i(t)$ in terms of the same quantities at time $t + \Delta t$,

$$\mathbf{r}_i(t) = \mathbf{r}_i(t+\Delta t) - \Delta t\mathbf{v}_i(t+\Delta t) + \frac{\Delta t^2}{2m_i}\mathbf{F}_i(t+\Delta t) + \mathcal{O}(\Delta t^3). \tag{3.6}$$

Using equation (3.5) for the first term in this expansion, we obtain

$$\mathbf{v}_i(t+\Delta t) = \mathbf{v}_i(t) + \frac{\Delta t}{2m_i}\left[\mathbf{F}_i(t) + \mathbf{F}_i(t+\Delta t)\right] + \mathcal{O}(\Delta t^2). \tag{3.7}$$

after some simple algebraic manipulations. Together, equations (3.5) and (3.7) provide a scheme to evolve locations and velocities of the particles at the same time. Note however that we need the intermolecular forces both at time t and $t+\Delta t$ to compute the velocity, such that we need some extra storage if we want to compute the forces only once per timestep. If we want to work memory-efficient, we should divide the velocity update into two steps, yielding the algorithm in Figure 3.5 for performing one time step.

velocity-Verlet Algorithm

1. $\mathbf{v} \leftarrow \mathbf{v} + \frac{\Delta t^2}{2m_i}\mathbf{F}$
2. $\mathbf{r} \leftarrow \mathbf{r} + \Delta t\mathbf{v}$
3. $\mathbf{F} \leftarrow \mathbf{F}(\mathbf{r})$
4. $\mathbf{v} \leftarrow \mathbf{v} + \frac{\Delta t^2}{2m_i}\mathbf{F}$.

Figure 3.5: The velocity-Verlet algorithm.

Note that with this procedure, the force also needs to be calculated once at the very beginning of the simulation.

Although it has been shown that this integration algorithm is not extremely accurate, it is very widely used. The reason is closely related to the approach on which the molecular dynamics technique is based. In fact, when evolving the system it is less important that we get every position and every velocity of every particle perfectly right than it is to keep the system close to the appropriate phase space. This means that the velocity Verlet scheme shows great long-term stability in this regard [2].

3.6 Sampling Quantities of Interest

3.6.1 Averaging of Macroscopic Quantities

We have already explained how macroscopic quantities are calculated in molecular dynamics simulations. We basically move the system forward in time, log the respective quantities of interest at each time step, and calculate the average at the end of the simulation. However, this is a bit simplified.

Since the positions and velocities of all the system particles at time $t + \Delta t$ depend on the respective quantities at time t, the derived macroscopic quantities will be correlated in some way. Therefore, since the calculation of a macroscopic quantity also consumes computational power, it might not be necessary to take every single step into account. Rather, one can move the system forward in time for several steps and then perform the next quantity evaluation.

3.6.2 Calculation of Correlation Functions

Furthermore, we are not only interested in simple observables, but also correlation function, which can in turn be related to further macroscopic quantities of the investigated system.

While we only need the current positions and velocities for the calculation of averages, we also need to know past positions and velocities for the correlation functions. In order to work memory-efficient here, one usually uses a ring buffer to store the respective values for easy calculation.

3.7 Thermostatting in Molecular Dynamics Simulations

The basic molecular dynamics technique is designed in such a way that it preserves the total energy of the system. As we have already learned, this situation is described by microcanonical ensembles. However, for canonical ensembles, we need to fix the temperature and let the total energy fluctuate according to the Boltzmann factor. It is therefore necessary to find a way to control the temperature during the time evolution of our simulated system. This procedure is called thermostatting and can be achieved with the help of various techniques.

Of course, a thermostat is an instrument to simulate the interaction of our physical system with the coupled heat bath. Since temperature is microscopically related to the kinetic energy of the particles, it is obvious that thermal regulation is obtained via rescaling of the velocities of the molecules. This step can conceptually be performed in two different ways, using either *deterministic* or *stochastic* methods. We will describe thermostats of either type in the following discussion. Note that all concepts for thermostats do not describe the actual physical processes occurring in temperature regulation of the canonical system, but are rather an instrument to guide the system through all accessible total energy shells consistent with a fixed temperature.

3.7.1 Nosé-Hoover (Chain) Thermostat

The Nosé-Hoover thermostat is a deterministic thermostat based on the findings of Nosé [52, 53] in the formulation of Hoover [36, 37]. In this method, an additional, fictitious degree of freedom representing the heat bath is introduced. This leads to an extended Hamiltonian with $6N + 2$ variables representing the combined system implemented as a microcanonical ensemble. It has been shown that the original $6N$ physical variables will then describe a system representing a canonical ensemble. Comparing the results obtained with the Nosé-Hoover thermostat to others, we see that static as well as dynamic system properties are not too far off from already validated data.

The Nosé-Hoover thermostat describes a system with one conservation law, i.e. the total energy of the extended Hamiltonian. If there are additional conservation laws to be applied to the system, stemming e.g. from external forces acting on the system, the resulting system behavior will be different. As a solution, it has been proposed to couple the system to another thermostat for each conservation law in place, yielding a *chain* of thermostats [45]. These additional thermostats each introduce further fictitious degrees of freedom that allow taking into account the additional constraints imposed on the system by the conservation laws. As a special case, it is even possible to attach one Nosé-Hoover thermostat to each particle, which

allows faster equilibration of the system and has turned to be very useful e.g. for proteins in aqueous solution [69].

3.7.2 Gaussian Thermostat – The Isokinetic Ensemble

The *Gaussian thermostat* inherits its name from the fact that the Gaussian principle of least constraint is employed to fix the total kinetic energy. The latter is the reason why the corresponding ensemble is called *isokinetic ensemble*. The equations of motion were first stated by Evans and Morriss [49], where the constraint was written as

$$\sum_{i=1}^{N} \frac{\mathbf{p}_i^2}{2m_i} = K, \tag{3.8}$$

yielding for the Hamiltonian

$$\dot{\mathbf{q}}_i = \frac{\mathbf{p}_i}{m_i}, \tag{3.9a}$$

$$\dot{\mathbf{p}}_\mathbf{i} = \mathbf{F}_i - \alpha \mathbf{p}_i. \tag{3.9b}$$

It is possible to find an explicit representation for the Lagrange multiplier α, which is given as

$$\alpha = \frac{\sum_{j=1}^{N} \mathbf{F}_j \frac{\mathbf{p}_j}{m_j}}{\sum_{j=1}^{N} \frac{\mathbf{p}_j^2}{m_j}}. \tag{3.10}$$

It turns out that compared to other methods, the isokinetic ensemble allows larger timesteps in the integration of the equations of motion, which is very favorable regarding the computational cost.

However, we need to note that the ensemble is slightly different from the canonical ensemble, as only the position coordinates are canonically distributed, while the momentum coordinates are constrained to one energy shell by definition. However, this difference appears to be very small, especially for large N. Furthermore, since the two parts of the partition function based on coordinates and momenta can be separated, one can easily relate the total canonical and isokinetic partition functions.

The Gaussian thermostat has been used in a part of the simulations.

3.7.3 Andersen Thermostat

The thermostat designed by Andersen [3] simulates random collisions of the physical system particles with particles of the heat bath, thereby changing their velocity. Therefore, after a certain number of steps (the frequency is given by the chosen strength of the coupling between system and heat bath) a number of system particles is chosen randomly and their velocities are resampled independently from a Maxwell-Boltzmann distribution corresponding to temperature T. This way, with each collision, the system is moved from one constant energy shell to another, in the end yielding a sampling over all accessible energy shells, which are ultimately weighted according to their Boltzmann factor.

The biggest advantage of the Andersen thermostat is its conceptual simplicity. It has been shown that it yields excellent results for the calculation of static quantities, e.g. equation-of-state data. However, since the thermostatting process does not reflect the occurring physical processes, but rather artificially changes the then discontinuous trajectories, the results related to dynamical parameters like the diffusion constant are poor, and their quality even decreases with increasing velocity resampling frequency.

3.7.4 Langevin Thermostat

The feasibility of Langevin thermostats in classical molecular dynamics simulations has been demonstrated by Bussi and Parinello in 2007 [8]. Ceriotti et al. have shown their implementation in PIMD and RPMD simulations [17].

For the Langevin thermostat, we consider the heat bath to consist of very many, very small particles. Therefore, collisions of a physical particle with a heat bath particle will happen frequently, but cause only a small change in the motion of the physical particle. For the physical system, these collisions can therefore be considered as small perturbations of the particle motion. Since we are not interested in the movement of the heat bath particles, we will not model them explicitly, but treat these perturbation in a statistical manner.

The use of Langevin dynamics leads to stochastic differential equations, namely

$$\mathrm{d}\mathbf{q}_i(t) = \frac{\mathbf{p}_i(t)}{m_i}\mathrm{d}t, \tag{3.11a}$$

$$\mathrm{d}\mathbf{p}_i(t) = \mathbf{F}_i(\mathbf{q}(t))\mathrm{d}t - \gamma\mathbf{p}_i(t)\mathrm{d}t + \sqrt{2m_i\gamma k_B T}\mathrm{d}W(t), \tag{3.11b}$$

where γ is a friction coefficient and $\mathrm{d}W(t)$ describes a Wiener noise, i.e. $\langle \mathrm{d}W(t) \rangle = 0$, $\langle \mathrm{d}W(t)\mathrm{d}W(t') \rangle = \delta(t - t')$. The implementation of this system of equations is performed via the following reformulation of the Hamiltonian,

$$\dot{\mathbf{q}}_i = \frac{\mathbf{p}_i}{m_i}, \tag{3.12a}$$

$$\dot{\mathbf{p}}_\mathbf{i} = \mathbf{F}_i - \gamma \mathbf{p}_i + \sigma \xi(t), \tag{3.12b}$$

where we used a fluctuation-dissipation relation for σ,

$$\sigma^2 = 2\gamma m_i k_B T. \tag{3.13}$$

The quantity ξ, which represents the Wiener noise from the stochastic differential equation, denotes an uncorrelated Gaussian random variable with zero mean and unit variance. This reformulation can interpreted as follows. The term including the γ describes additional friction in the system, while the random force represented by the term including ξ describes the unpredictable collisions with the heat bath.

Further details on the implementation of the Langevin thermostat will be discussed later on in Chapter 6.

3.8 Conclusions

Based on the essential requirement of a suitable interaction model, the classical equations of motion is a very good approximation for most materials, where also good agreement is seen with experiments. However, when it comes to light particles (like H_2 or D_2, which we will consider in this thesis), low temperatures, or high vibrational frequencies, quantum effects play an important role and cannot be neglected any more. Fortunately, the molecular dynamics simulation method can be generalized to allow the investigation of quantum mechanical systems. Since we are interested in D_2 at low temperatures, we need to draw our attention to these methods in the following chapters.

Chapter 4

The Path Integral Formalism

Starting at the beginning of the twentieth century, when the experiments on the blackbody spectrum of electromagnetic radiation led to disturbing results, it became clear that the classical model of nature was wrong under certain circumstances. Based on experiments showing the photoelectric effect as well as those showing interference patterns of light, a theory emerged that postulates the wave-particle duality as well as the quantization of observables: *quantum mechanics*.

The theory of quantum mechanics, in particular the uncertainty principle, prohibits a simultaneous arbitrarily exact measurement of, e.g. a particle's position and momentum, thereby destroying the deterministic view of physics. (Physicists say that position and momentum do not *commute*.) Rather, in the Schrödinger picture, it moves to a description of a system as a *wave function*, which carries the whole information. If we now do know certain commuting physical parameters of the system, we need to choose the related space representation for the wave function. Then, the probabilities for parameters that cannot be measured at the same time, can be computed using the absolute square of the wave function.

Furthermore, while in classical mechanics, the transition of a system's state S_A at time t_0 to a state S_B at time t_1 is deterministically defined, this is not the case in quantum mechanics.

There are many possible paths for the evolution of the system between t_0 and t_1 that are compatible, and each of those paths is taken with a certain probability that depends on the amplitude of the wave function. This is shown in the sketch in Figure 4.1. If we now want to sample states of the system between t_0 and t_1, we need to take into account each of the possible paths and its likelihood in order to predict the respective outcome correctly. This is the heuristic basis for the *path integral formulation* which was introduced by Richard Feynman in 1948 [26].

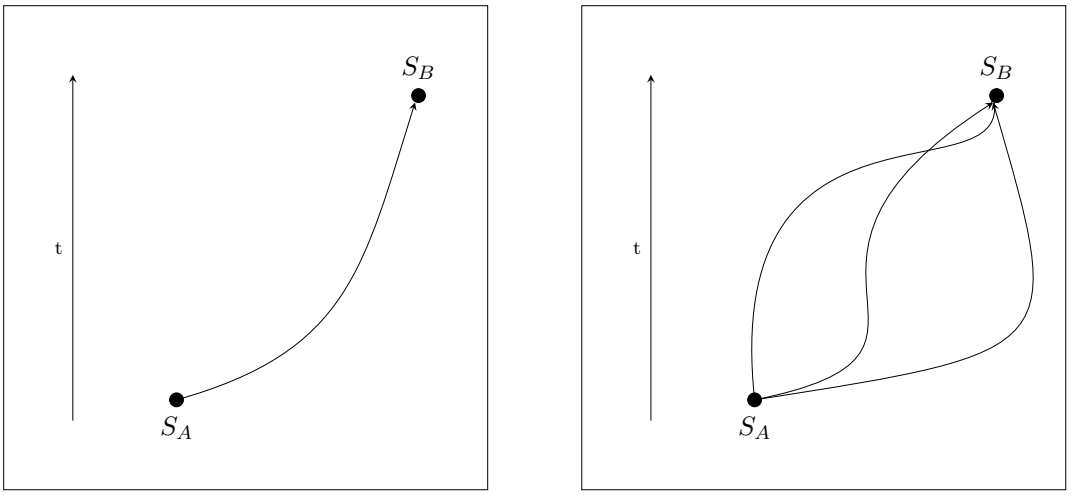

Figure 4.1: Sketch of (a) the classically and (b) *some* quantum mechanically possible paths between S_A and S_B.

In this chapter, we first formally derive the path integral formulation using the basic quantum statistical mechanics from Chapter 2, and discuss some inherent features. The derivation there is mainly based on the presentations in [70] and [20]. The following Section 4.2 addresses the implementation using a Monte Carlo approach, leading to the *Path Integral Monte Carlo* (PIMC) method.

4.1 Formal Derivation

For the derivation of the path integral formulation, we restrict ourselves to one particle in one dimension for the sake of simplicity and notation. The generalization to many particles and three dimensions is straightforward, and will only be briefly mentioned.

Let us recall the description of the quantum mechanical canonical ensemble described in Chapter 2. We start out with a coordinate space representation for the quantum states, which allows to write the density matrix as

$$\rho(x', x; \beta) = \left\langle x' \middle| \mathrm{e}^{-\beta\mathcal{H}} \middle| x \right\rangle . \tag{4.1}$$

Remembering that the Hamiltonian for the system is

$$\hat{\mathcal{H}} = \frac{\hat{p}^2}{2m} + U(\hat{x}) = \hat{K} + \hat{U}, \tag{4.2}$$

where $\hat{K}$ is the operator for the kinetic energy and $\hat{U}$ is the one for the potential energy, it appears to be useful to decompose the density operator with respect to $\hat{K}$ and $\hat{U}$. Unfortunately, since $\hat{K}$ contains the momentum operator and $\hat{U}$ contains the position operator, it turns out that those two do not commute. This prevents a straightforward application of that strategy. However, this drawback is overcome by considering the exact relation

$$\mathrm{e}^{-\beta\hat{\mathcal{H}}} = \left(\mathrm{e}^{-\beta_P(\hat{K}+\hat{U})}\right)^P, \tag{4.3}$$

where we have defined $\beta_P := \beta/P$, and then making use of the Trotter factorization,

$$\mathrm{e}^{-\beta_P(\hat{K}+\hat{U})} \approx \mathrm{e}^{-\beta_P\hat{U}/2}\mathrm{e}^{-\beta_P\hat{K}}\mathrm{e}^{-\beta_P\hat{U}/2}, \tag{4.4}$$

which is exact in the limit $P \to \infty$ [64], and the right hand side converges as $\mathcal{O}\left(P^{-2}\right)$. The number P is called *Trotter number*. With this, the density matrix in the coordinate space representation can therefore be written as

$$\rho(x', x; \beta) = \lim_{P\to\infty} \left\langle x' \middle| \left(\mathrm{e}^{-\beta_P\hat{U}/2}\mathrm{e}^{-\beta_P\hat{K}}\mathrm{e}^{-\beta_P\hat{U}/2}\right)^P \middle| x \right\rangle . \tag{4.5}$$

To proceed, we can now insert $(P-1)$ identity operators in terms of the coordinate space states

$$\hat{I} = \int \mathrm{d}x \, |x\rangle \langle x| \tag{4.6}$$

between successive factors, yielding

$$\begin{aligned}\rho(x', x; \beta) &= \lim_{P\to\infty} \int \mathrm{d}x^{(1)} \dots \mathrm{d}x^{(P-1)} \, \langle x'|\mathrm{e}^{-\beta_P\hat{\mathcal{H}}}|x^{(1)}\rangle \, \langle x^{(1)}|\mathrm{e}^{-\beta_P\hat{\mathcal{H}}}|x^{(2)}\rangle \dots \langle x^{(P-1)}|\mathrm{e}^{-\beta_P\hat{\mathcal{H}}}|x\rangle \\ &= \lim_{P\to\infty} \int \mathrm{d}x^{(1)} \dots \mathrm{d}x^{(P-1)} \rho(x', x^{(1)}; \beta_P)\rho(x^{(1)}, x^{(2)}; \beta_P) \dots \rho(x^{(P-1)}, x; \beta_P).\end{aligned} \tag{4.7}$$

This means that the canonical density matrix at temperature T can be expressed in terms of a product of canonical density matrices at temperature $P \cdot T$. This comes in handy since the application of the Trotter formula requires a certain temperature such that the error does not grow beyond an acceptable size. The big advantage of this representation is that the considered states $\left|x^{(i)}\right\rangle$ are eigenvectors of the potential energy operator, which allows to replace the operator by its corresponding eigenvalue, such that we then obtain (for one single term)

$$\langle x^{(k)}|\mathrm{e}^{-\beta_P \hat{U}/2}\mathrm{e}^{-\beta_P \hat{K}}\mathrm{e}^{-\beta_P \hat{U}/2}|x^{(k+1)}\rangle = \mathrm{e}^{\beta_P U(x^{(k)})/2}\,\langle x^{(k)}|\mathrm{e}^{-\beta_P \hat{K}}|x^{(k+1)}\rangle\,\mathrm{e}^{-\beta_P U(x^{(k+1)})/2}. \quad (4.8)$$

Now, we are left with an operator depending on the momentum, but acting on coordinate space states, which prevents an immediate evaluation. In order to enable the evaluation of the momentum operator, we can again insert identity operators, but here in terms of momentum space states in a similar manner as before,

$$\hat{I} = \int \mathrm{d}p\,|p\rangle\,\langle p|\,, \quad (4.9)$$

such that for the involved matrix element, we arrive at

$$\begin{aligned}\langle x^{(k)}|\mathrm{e}^{-\beta_P \hat{K}}|x^{(k+1)}\rangle &= \int \mathrm{d}p\,\langle x^{(k)}|\mathrm{e}^{-\beta_P \hat{K}}|p\rangle\;\langle p|x^{(k+1)}\rangle \\ &= \int \mathrm{d}p\,\langle x^{(k)}|p\rangle\;\langle p|x^{(k+1)}\rangle\,\mathrm{e}^{-\beta_P p^2/2m} = (*).\end{aligned} \quad (4.10)$$

The remaining inner products can also be evaluated using

$$\langle x|p\rangle = \frac{1}{\sqrt{2\pi\hbar}}\mathrm{e}^{ipx/\hbar}, \qquad \langle p|x\rangle = \frac{1}{\sqrt{2\pi\hbar}}\mathrm{e}^{-ipx/\hbar}, \quad (4.11)$$

yielding

$$\begin{aligned}(*) &= \frac{1}{2\pi\hbar}\int \mathrm{d}p\,\mathrm{e}^{-\beta_P p^2/(2m)}\mathrm{e}^{ip\left[x^{(k)}-x^{(k+1)}\right]/\hbar} = \\ &= \frac{1}{2\pi\hbar}\mathrm{e}^{-m\left[x^{(k)}-x^{(k+1)}\right]^2/(2\beta_P\hbar^2)}\int \mathrm{d}p\,\mathrm{e}^{-\beta_P\left[p-im\left[x^{(k)}-x^{(k+1)}\right]/(\hbar\beta_P)\right]^2/(2m)} = \\ &= \sqrt{\frac{m}{2\pi\beta_P\hbar^2}}\mathrm{e}^{-m\left[x^{(k)}-x^{(k+1)}\right]^2/(2\beta_P\hbar^2)},\end{aligned} \quad (4.12)$$

where we have completed the square at the second equal sign. Summarizing all these calculations and inserting their results into equation (4.1), the density matrix reads

$$\rho(x', x; \beta) = \lim_{P\to\infty}\left(\frac{m}{2\pi\beta_P\hbar^2}\right)^{P/2}\int \mathrm{d}x^{(2)}\cdots\mathrm{d}x^{(P)}\,\mathrm{e}^{-\beta_P\phi_P(x)}, \quad (4.13)$$

where

$$\phi_P(x) := \phi(x^{(1)}, \ldots, x^{(P)}) = \sum_{k=1}^{P} \left[\frac{m}{2} \omega_P^2 \left(x_k - x_{k+1} \right)^2 + U(x_k) \right] \Bigg|_{x_1 = x, x_{P+1} = x'} \tag{4.14}$$

and

$$\omega_P := \frac{1}{\beta_P \hbar}. \tag{4.15}$$

For one particle in one dimension, we can then write the canonical partition function as

$$Q(T) = \mathrm{Tr}\left[\mathrm{e}^{-\beta \mathcal{H}} \right] = \int \mathrm{d}x \, \rho(x, x; \beta), \tag{4.16}$$

which means that the end point of the path is identical with the initial point. Straightforwardly, based on equation (2.13), the expected value for operators solely depending on the position can be written as

$$\begin{aligned} \langle A \rangle &= \frac{1}{Q} \int \mathrm{d}x \; \langle x | \rho(x, x; \beta) \hat{A} | x \rangle \\ &= \lim_{P \to \infty} \frac{1}{Q_P} \left(\frac{m}{2\pi \beta_P \hbar^2} \right)^{P/2} \int \mathrm{d}x \, \mathrm{e}^{-\beta_P \phi_P(x)} A_P(x), \end{aligned} \tag{4.17}$$

where Q_P is the partition function based on the density matrix with finite P, and where

$$A_P(x) = \frac{1}{P} \sum_{k=1}^{P} A(x^{(k)}). \tag{4.18}$$

Note that due to the equality of initial and final state of the density matrix for the partition function and the expected value, we define $P + 1 \equiv 1$ in equation (4.14). This assumption will be made throughout the rest of this thesis.

With this, we have formally arrived at representations for the quantum mechanical canonical partition function as well as for thermodynamic observables depending on position. But what does this have to do with path integrals? The link is a relation between the canonical density matrix and the quantum mechanical time propagator, given by

$$\hat{U}(t) = \mathrm{e}^{-i\mathcal{H}t/\hbar}. \tag{4.19}$$

Due to the obvious relationship

$$\hat{\rho}(\beta) = \mathrm{e}^{-\beta \mathcal{H}} = \hat{U}(-i\beta\hbar), \tag{4.20}$$

we can consider the density matrix operator as an *imaginary time propagator*, propagating a state by time $-i\beta\hbar$. Therefore, our derivation, in particular equations (4.13) and (4.17), represent a path integral in imaginary time, having common initial and final points. By splitting the Boltzmann factor into P parts, we create $P-1$ time points separated in imaginary time, allowing to consider the whole expression derived in equation (4.16) as the partition function of a closed ring polymer.

The representation in equation (4.17) therefore allows to interpret the quantum mechanical expected value for one particle in one dimension as an expected value for a *classical* ring polymer with an alternative potential given by $\phi_P(x)$ in (4.14). This close connection between the classical and quantum mechanical description of such a system has been termed *classical isomorphism* [18].

Remark
Although this derivation is only exact in the limit $P \to \infty$, it turns out that in computer simulations it is often enough to choose P to be in the range of 10^2 when using the potential given in equation (4.14). Furthermore, there are also more accurate (but therefore more complicated) approximations to the density matrix that do not require more than 10 monomers.

Obviously, the involved potential $\phi_P(x)$ includes harmonic spring forces between neighboring monomers, which are frequently called *beads*. Let us therefore have another look at the related spring constant defined in equation (4.14). For low temperatures as well as for small masses, its numerical value is also small, yielding weaker forces between the neigbouring atoms, which results in larger mean distances between the beads of one polymer. For higher temperatures and larger masses, however, the spring forces become stronger and stronger, yielding lower distances between the beads of the polymer, until, in the classical limit, all beads coincide and therefore just represent the classical particle. This fact also shows that the path integral formalism is a generalization of the classical model.

Extending this formulation to many quantum mechanical particles is mostly straightforward. However, there is one important difference to the truly classical case. While in the case of genuine classical polymers, there will be an interaction between every atom present in the system, this is not the case for the path integral case. Here, each bead only interacts with its two neighbors on the same ring polymer, and furthermore with the beads of the same index on all the other ring polymers, while there is no interaction with the rest of the beads.

4.2 Simulation Techniques – Path Integral Monte Carlo

We now need to transform this theoretical derivation of the path integral formulation into a practical implementation for the simulation of quantum mechanical systems. Since the expression in equation (4.14) only contains a configurational partition function,

$$Q = \lim_{P\to\infty} \left(\frac{m}{2\pi\beta_P\hbar^2}\right)^{P/2} \int \mathrm{d}x\, \mathrm{e}^{-\beta_P \phi_P(x)}, \tag{4.21}$$

the first thing that comes to mind is to use a generalization of the Monte Carlo method, where we do not consider an actual dynamical movement. This *path integral Monte Carlo* (PIMC) method has been used for various quantum mechanical systems. The best efficiency has been found for Boltzmann systems, but there are no principal problems for Bose and Fermi systems [6, 68], although some practical challenges arise within the implementation. However, it is still an excellent choice for the calculation of equilibrium properties. For this reason, the PIMC method has been thoroughly investigated for its applicabilities as well as strengths and weaknesses compared to other techniques [16].

As we have seen, in the path integral formulation the interactions are slightly different compared to a truly classical ring polymer. On the one hand, each bead interacts with its two neighbors on the same ring polymer, where harmonic potentials are assumed. On the other hand, it interacts with each bead of the same index in all other ring polymers. Here, an appropriate intermolecular potential is used. A sketch of the interactions between the involved particles is shown in Figure 4.2.

Apart from having P times as many particles in the whole system, the main difficulty compared to classical Monte Carlo simulations is that for large numbers of beads P the usual acceptance rates for the trial moves are extremely low, which leads to a very low convergence rate. The reason for the low acceptance rates is based on the fact that the stiff springs between the beads only allow very small changes in the relative monomer configuration at each step. A naive solution to this is to move polymers as a whole, and to combine this with small monomer moves.

More sophisticated methods to overcome those problems are the so-called *staging* [56] and *normal mode transformations* [71]. However, even using those it is necessary to not move a whole ring polymer per step, but rather only operate segments of a polymer at a time, which increases the acceptance rates, and hence efficiency.

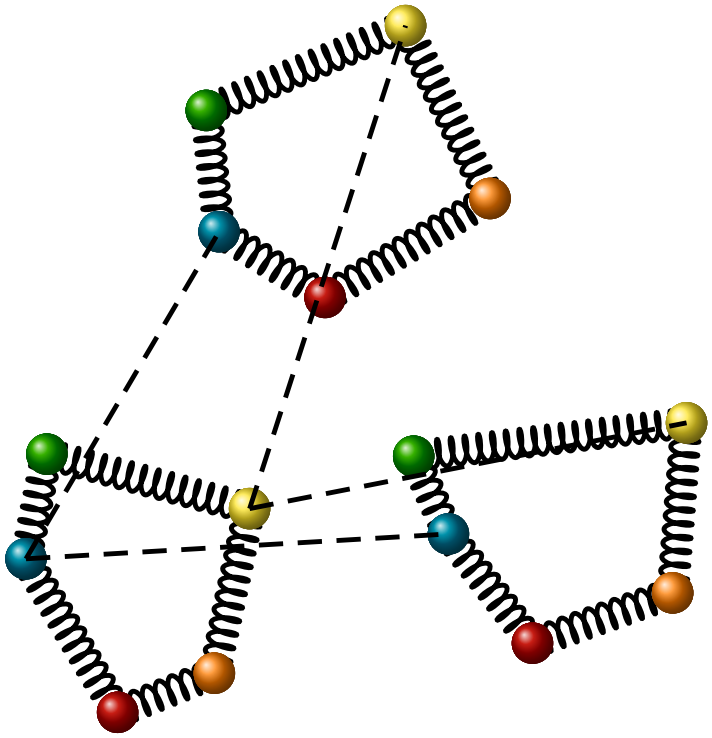

Figure 4.2: Interactions between the beads of several ring polymers. The springs represent the harmonic potentials, while the dashed lines represent the intermolecular potential. Note that each bead only interacts with a single bead of each other molecule.

4.3 Conclusions

The use of the classical equations of motion is a very good approximation for a lot of materials, where also good agreement is seen between simulations and experiments. However, when it comes to light particles (like H_2 or D_2, which we will consider in this thesis), low temperatures, or high vibrational frequencies, quantum effects play an important role and cannot be neglected any more. Fortunately, the use of the path integral formalism – as we have derived it in this chapter – allows a neat way to treat quantum mechanical systems. The approach allows to deal with a quantum mechanical system in a similar way as with classical systems, albeit with a different Hamiltonian, hence the term *classical isomorphism*.

We have also seen a first approach to implement such systems, but, similarly to the classical case, MC simulations do not provide dynamical information. Therefore, the obvious solution is to devise a generalization of the MD method to quantum mechanical systems, which will be able to handle this task. This will be the topic of the following chapter.

Chapter 5

Molecular Dynamics Simulations Based on the Path Integral Formalism – The RPMD Method

We will now discuss the implementation of molecular dynamics methods based on the path integral formulation. These methods can be derived from the results of the previous chapter, where we obtained expressions depending only on the system configuration, which was sufficient for the implementation of the Monte Carlo method. To use MD simulations, we need to include momentum information to enable the propagation of the system and the evaluation of dynamical properties. This adaption is presented in Section 5.1. Note again that while the PIMC method as well as all MD methods under discussion here provide an in principle exact calculation for static properties, the results for dynamical properties can only be obtained from MD simulations, and those are only approximate.

We will then present and discuss several molecular dynamics methods to simulate systems based on the classical isomorphism. Each of them incorporates a different approach and is favorable under certain conditions or for certain objectives, but also has its drawbacks, such

that there exists no general method of choice. We end Section 5.1 with the description of the basic path integral molecular dynamics method (PIMD), then briefly describe the centroid molecular dynamics method (CMD) in Section 5.2. The last approach to be discussed is the ring polymer molecular dynamics (RPMD) method in Section 5.3, which is also the implementation investigated in this thesis.

5.1 Adapting the Classical Isomorphism Result for Molecular Dynamics Simulations – Path Integral Molecular Dynamics

Although we obtained a nice classical-like Boltzmann probability density as a weight factor in the partition function in Chapter 4, we note again that this only covers the configurational part. Since we cannot simulate the physical propagation of the system in time without any information on the momenta, we need to extend the Boltzmann factor in some way such that $\mathbf{p}$ enters the expression. Of course, the strategy is again to add a representation of the identity involving the desired quantities.

We will again restrict the system to one quantum mechanical particle for the sake of notational simplicity, where the generalization to a many-body system in three dimensions is easily obtained in a straightforward manner.

The idea is to insert a normalized Gaussian integral of the form

$$\left(\frac{\beta_P}{2m'\pi}\right)^{P/2} \int \mathrm{d}p\, \mathrm{e}^{-\beta_P \sum_{k=1}^{P} p_k^2/2m'} = 1 \tag{5.1}$$

containing a fictitious mass m' into equation (4.17) to obtain

$$\langle A \rangle = \lim_{P\to\infty} \frac{1}{Q} \frac{1}{(2\pi\hbar)^P} \left(\frac{m}{m'}\right)^{P/2} \int \mathrm{d}x\mathrm{d}p\, \mathrm{e}^{-\beta_P \mathcal{H}_P(x,p)} A_P(x). \tag{5.2}$$

With this reformulation, the Boltzmann factor comprises a full Hamiltonian for a single ring polymer, namely

$$\mathcal{H}_P(x,p) = \sum_{k=1}^{P} \left[\frac{p_k^2}{2m'} + \frac{m}{2}\omega_P^2 \left(x_k - x_{k+1}\right)^2 + U(x_k)\right]. \tag{5.3}$$

This is the expression that will form the basis for our methods for the evolution of our quantum mechanical system in time. With this, the simulation basically works as in the classical case, where the only difference is again the action of the intermolecular potential between the beads of the same index, as has already been discussed in Chapter 4.

Note however that the mass m' introduced within the momentum expression has nothing to do with the physical mass m of the particles, and is completely arbitrary. Rather, it only determines the rate at which the system evolves dynamically in time. Therefore, in general PIMD simulations, it is natural to choose it in a way such that the sampling process is most efficient. While this technique appears to be very favorable for the calculation of static properties, the lack of physical correspondence of m' still prevents the *direct* calculation of any dynamic parameters. This drawback is overcome by other methods like centroid molecular dynamics as well as by ring polymer molecular dynamics, which will be discussed in the following sections.

5.2 Centroid Molecular Dynamics

The centroid molecular dynamics (CMD) method originates from the findings published by Cao and Voth [9, 10, 11, 12, 13]. It is based on the definition of the so-called *path centroids*, which, in the discretized path integral formulation, are equal to the centers of mass of each quantum particle (i.e. of the ring polymer). We will again present this method for one particle in one dimension for the sake of notational simplicity.

For an Euclidean path, the imaginary time action functional for a particle of mass m, experiencing a potential V is given by [35]

$$S\left[p(\tau), x(\tau)\right] = \int_0^{\hbar\beta} \mathrm{d}\tau \left[-ip(\tau)\frac{\mathrm{d}x(\tau)}{\mathrm{d}\tau} + \frac{m}{2}\left(\frac{\mathrm{d}x(\tau)}{\mathrm{d}\tau}\right)^2 + U\left(x(\tau)\right)\right]. \tag{5.4}$$

The *centroid variables* are here defined by integration over imaginary time, namely

$$x_0 = \frac{1}{\hbar\beta}\int_0^{\hbar\beta} \mathrm{d}\tau\, x(\tau), \qquad p_0 = \frac{1}{\hbar\beta}\int_0^{\hbar\beta} \mathrm{d}\tau\, p(\tau). \tag{5.5}$$

Using those, the partition function can be written as an integral of the imaginary time action integral over all closed centroid constrained paths and over all possible centroid configurations, yielding

$$\begin{aligned} Q &= \frac{1}{\hbar}\int \mathrm{d}x_c\, \mathrm{d}p_c \int \mathrm{d}x(\tau)\, \mathrm{d}p(\tau)\, \delta(x_c - x_0)\delta(p_c - p_0)\mathrm{e}^{-S[p(\tau),x(\tau)]/\hbar} \\ &= \int \mathrm{d}x_c\, \mathrm{d}p_c \int \mathrm{d}x(\tau)\, \mathrm{d}p(\tau)\, \rho_c(p_c, x_c), \end{aligned} \tag{5.6}$$

where the corresponding centroid distribution function is given by

$$\rho_c(p_c, x_c) = \mathrm{e}^{-\beta p_c^2/2m}\mathrm{e}^{-\beta V_c(x_c)}. \tag{5.7}$$

Here, V_c is the potential of mean force. For the evolution of the system in time, we use the classical equations of motion for the centroid variables

$$\dot{x}_c = \frac{p_c}{m} \qquad \dot{p}_c = -\frac{\mathrm{d}V_c}{\mathrm{d}x_c}, \tag{5.8}$$

where the *centroid force* can be written as

$$\frac{\mathrm{d}V_c}{\mathrm{d}x_c} = \frac{1}{\rho_c}\int \mathrm{d}x(\tau)\mathrm{d}p(\tau)\delta(x_c - x_0)\delta(p_c - p_0)\frac{\mathrm{d}V(x)}{\mathrm{d}x}\mathrm{e}^{-S[p(\tau),x(\tau)]/\hbar}. \tag{5.9}$$

With this, centroid averages are calculated via

$$\langle A\rangle = \frac{1}{hQ}\int \mathrm{d}p_c\mathrm{d}x_c\,\rho_c(p_c, x_c)A_c(p_c, x_c), \tag{5.10}$$

while centroid correlation functions are similarly obtained from

$$\langle A_c(0)B_c(t)\rangle = \frac{1}{hQ}\int \mathrm{d}p_c\mathrm{d}x_c\,\rho_c(p_c, x_c)A_cB_c(t), \tag{5.11}$$

where $B_c(t) := B(p_c(t), x_c(t))$. It is important to mention the difference in the definition of the observable average compared to the PIMD method. While one needs to calculate the average over the observable values at the bead positions in PIMD, one calculates the observable value at the mean of the positions (i.e. the centroid),

$$A_c = A\left(\frac{1}{P}\sum_{k=1}^{P} x^{(k)}\right) \tag{5.12}$$

in the CMD method. The same goes, of course, for correlation functions.

Equation (5.11) is a well-defined approximation to the Kubo-transformed correlation function if at least one of the involved operators is a linear function of position or momentum, which has already been discussed in Chapter 2. In particular, the CMD method is exact for $t = 0$, for harmonic potentials (at all times), and in the classical limit [20]. It is also important to note that the centroid molecular dynamics method is able to capture dominant quantum many-body features like *zero-point effects* and *tunneling* [35].

The CMD method has been applied to calculate quantum effects in liquid para-hydrogen, liquid ortho-deuterium or liquid water. It turned out to be also very useful in the computation of vibrational spectra.

One important drawback of CMD, apart from the required linearity of the operator in x or p, is its computational cost. In particular, the integration of the equations of motion requires the calculation of the centroid forces given by equation (5.9). This would seem to require a full path integral simulation at each timestep, which yields a huge computational burden. A variant involving an adiabatic approximation lowers this computational burden [34].

5.3 Ring Polymer Molecular Dynamics

The ring polymer molecular dynamics (RPMD) method has been introduced by Craig and Manolopoulos [21], and has been thoroughly studied and applied to the calculation of dynamical system parameters since then [17, 20, 22, 30, 34, 48, 63]. The idea here is to overcome the lack of physical intuition introduced by the arbitrarily chosen fictitious mass m' in the momentum term. As might easily be guessed, the necessary step for this is the choice

$$m' = m, \tag{5.13}$$

such that each bead of the polymer has exactly the same mass as a single physical particle under consideration. This overcomes the non-physical propagation in a natural way, albeit for the price of a lower sampling efficiency compared to basic PIMD, as has been discussed earlier in this chapter. With this, the interpretation of the quantum particles as classical ring polymers with the already discussed interaction pattern is perfectly valid, and we can simply extend the Hamiltonian given in equation (5.3) to N molecules and propagate the system. The Hamiltonian then reads

$$\mathcal{H}_P^N(\boldsymbol{x}, \boldsymbol{p}) = \sum_{i=1}^{N} \sum_{k=1}^{P} \left[\frac{\left[p_i^{(k)}\right]^2}{2m} + \frac{m}{2}\omega_P^2 \left(x_i^{(k)} - x_i^{(k+1)} \right)^2 + U(\boldsymbol{x}) \right]. \tag{5.14}$$

The equations of motion are therefore given by

$$\dot{x}_i^{(k)} = \frac{p_i^{(k)}}{m}, \tag{5.15a}$$

$$\dot{p}_i^{(k)} = -m\omega_P^2 \left(2x_i^{(k)} - x_i^{(k+1)} - x_i^{(k-1)} \right) - \frac{\partial U(\boldsymbol{x})}{\partial x_i^{(k)}}. \tag{5.15b}$$

Note that in this setting, the equivalent classical simulation will be performed at a temperature of $P \cdot T$ instead of T, which is a typical choice for path integral simulations.

As for the classical case, by integrating equations (5.15) the total energy of the system is conserved, yielding a microcanonical ensemble. In order to obtain a canonical ensemble, we need to use a thermostat.

When implementing a thermostat, we still try to optimize the sampling procedure, in the sense that we would like to choose the coupling strength such that we explore the different energy shells most efficiently. In a Langevin thermostat, the coupling strength appears as the friction coefficient γ (see equation (3.11b)). For a harmonic oscillator, of which we have many in our system, it turns out that the best coupling strength depends on the respective eigenfrequency. The optimal strategy is therefore to couple each bead with its own thermostat. Further details on the coupling will be given in the following chapter, after we have introduced a useful method to exactly propagate the system under the free Hamiltonian, i.e. without any potential and without a thermostat.

Another aspect that needs to be discussed is dealing with the correlation functions. We have already mentioned that the RPMD method only approximates quantum mechanical correlation functions. In particular, this is only possible for operators involving position-dependent operators, where one usually computes the Kubo-transformed correlation function. It has been shown that this approximation becomes exact in two limiting cases:

- *The classical limit:* As we have already discussed earlier, in the classical limit, the strong spring forces cause all beads to be at the very same spot, which is identified with the position of the classical particle. In this case, the agreement with classical dynamical quantities is obvious.
- *The harmonic limit:* In his dissertation, Craig [20] showed the coincidence of the RPMD approximation with the exact solution for harmonic external potentials in connection with linear operators of the position under consideration.

The definition of expected values and correlation functions for RPMD method is similar to the PIMD method, i.e.

$$\langle A \rangle = \frac{1}{Q} \frac{1}{(2\pi\hbar)^P} \int \mathrm{d}x \mathrm{d}p \, \mathrm{e}^{-\beta_P \mathcal{H}_P(x,p)} \frac{1}{P} \sum_{k=1}^{P} A(x^{(k)}) \tag{5.16a}$$

$$\langle A(0)B(t) \rangle = \frac{1}{Q} \frac{1}{(2\pi\hbar)^P} \int \mathrm{d}x \mathrm{d}p \, \mathrm{e}^{-\beta_P \mathcal{H}_P(x,p)} \frac{1}{P} \sum_{k=1}^{P} A(x^{(k)}(0)) B(x^{(k)}(t)). \tag{5.16b}$$

Our main interest in this thesis lies in the calculation of the velocity autocorrelation function $C_{vv}(t)$, which then allows to calculate the diffusion constant D of a liquid via

$$D = \frac{1}{3}\int_0^\infty \mathrm{d}t\, C_{vv}(t) = \frac{1}{6}\int_{-\infty}^\infty \mathrm{d}t\, C_{vv}(t). \tag{5.17}$$

At first glance, its calculation seems to be beyond the capabilities of the RPMD method, since no position-dependent operator is involved. What saves the day here is the fact that the velocity autocorrelation function is directly related to the position autocorrelation function via

$$C_{vv}(t) = -\frac{\mathrm{d}^2 C_{xx}(t)}{\mathrm{d}t^2}, \tag{5.18}$$

yielding

$$C_{vv}(t) = \frac{1}{Q}\int \mathrm{d}\boldsymbol{x}\mathrm{d}\mathbf{p}\, \mathrm{e}^{-\beta_P H_P(\mathbf{p},\boldsymbol{x})} v_P(t) v_P(0), \tag{5.19}$$

where v_P is defined analogeously to equation (4.18).

Note that the RPMD method only *mimics* physical motion, which allows the calculation of dynamical system properties. However, the ring polymer dynamics do not correspond in any way to actual quantum system dynamics [20]. As a consequence, real-time quantum interference effects are not covered by this method. The importance of the RPMD method is saved by the fact that for many condensed phase systems these effects can be neglected.

The big advantage of RPMD methods over CMD methods is the much lower computational cost. The RPMD method has been successfully applied in investigations on various systems. Starting with liquid para-hydrogen, which is kind of a benchmark system, the importance of quantum mechanical effects in liquid dynamics has been demonstrated [48]. Similarly encouraging results have been obtained in the study of liquid water [19, 31]. Moreover, RPMD covers zero point energy effects in many different systems, ranging from water to ice [43] to binary supercooled liquids near glass transition [44]. RPMD applicability is rounded off by reproducing tunneling effects in chemical dynamics [22].

5.4 Conclusions

This chapter shed light on feasible methods to computationally investigate dynamical properties of quantum mechanical systems. As discussed, each of the mentioned methods shows

advantages as well as drawbacks, which does not put one approach in ahead of the others. Rather, one needs to choose the most suitable method according to the system and to the observable one is interested in.

Chapter 6

Methods

We are now almost ready for the simulation of quantum mechanical systems. The final missing piece of the puzzle consists of details on the implementation. Therefore, this chapter is devoted to the description and explanation of the methods implemented. In particular, we will discuss the interatomic potential employed to model D_2, the *Silvera-Goldman* potential, in Section 6.1. Then, we explain the use of normal coordinates in Section 6.2, which allow an exact evolution of the system under the free Hamiltonian. This discussion is based on [17]. With this, we are ready to describe the actual algorithm used for our computations in Section 6.3. The chapter ends with a description of the computational parameters used.

6.1 The Silvera-Goldman Potential

When performing molecular dynamics simulations, a delicate task is the choice of the intermolecular potential. The calculation of the molecular interaction can only be performed *ab initio* for very simple system, and even then, it is quite costly. For complicated systems, this might not be possible at all, which is why in this case that step of the procedure is heavily based on empirical work. As a consequence, there are many different types of potentials, all

trying to capture the specificities of the system under consideration. Typically, simple analytic ansatz functions comprising free parameters are chosen, which can then be adapted to fit theoretical or experimental data. As an example, the most simple one, the Lennard-Jones potential has already been discussed previously in Section 3.4. However, Silvera and Goldman derived another type of potential which appears to be more suitable for the description of the intermolecular forces in ortho-deuterium [65], and has been shown to yield excellent agreement with experimental results. The *Silvera-Goldman potential* will also be employed throughout this thesis, and is written as

$$U(r) = \mathrm{e}^{\alpha-\beta r-\gamma r^2} - \left(\frac{C_6}{r^6} + \frac{C_8}{r^8} - \frac{C_9}{r^9} + \frac{C_{10}}{r^{10}}\right) \cdot f_c(r), \tag{6.1}$$

where

$$f_c(r) = \begin{cases} \mathrm{e}^{-\left(\frac{1.28 r_c}{r}-1\right)^2} & r \leq r_c, \\ 1 & r > r_c. \end{cases} \tag{6.2}$$

The first, exponential, term describes the intermolecular repulsion at close distances, while the second part of the potential is the dispersion interaction, as modeled by the coefficients C_6, C_8, and C_{10}, which also gives rise to the potential well at around 0.344 nm. A noteworthy feature here is the introduction of the C_9/r^9 term, which is meant to account for the repulsive three-body tripole-dipole dispersion interaction [65]. The function f_c is a damping function that prevents $U(r)$ from becoming singular for $r \to 0$. Altogether, this means that the Silvera-Goldman potential is an effective pair potential that also incorporates many-body interactions.

The numerical values of the involved parameters are given in Table 6.1, and the shape of the potential is presented in Figure 6.1, where also a comparison to the best available fit of the Lennard-Jones potential for solid D_2 (albeit for a higher temperature regime) is shown. The values for the latter (ε/k_B=37 K, $\sigma = 0.2928$ nm) are taken from [41]. It is obvious that despite the qualitative similarity, the equilibrium distance between two particles is a little higher for the Silvera-Goldman potential (0.344 nm compared to 0.329 nm for the Lennard-Jones potential), which will certainly create different results in the simulations.

At the end of this description it is once again noted that this potential only describes the interaction of a bead of one given ring polymer with the corresponding beads of the same index on the other ring polymers. The interactions between beads of the same ring polymer are modeled as springs, and therefore harmonic potentials, while there is no interaction with beads with different indices in other ring polymers.

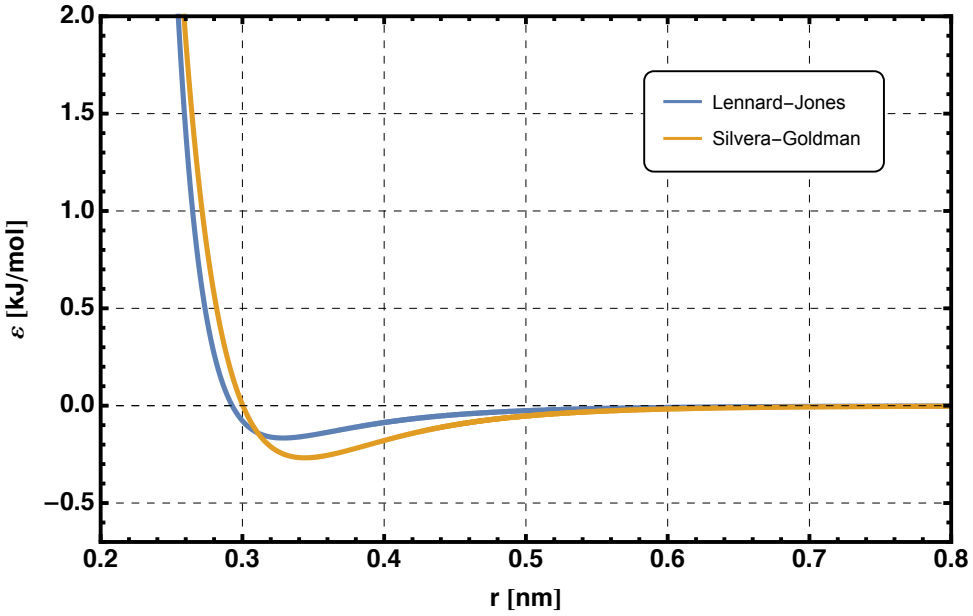

Figure 6.1: The shape of the Silvera-Goldman potential, compared to the best available fit for the Lennard-Jones potential for D_2.

Parameter	Value	Parameter	Value
α	1.713	C_6	12.14
β	1.5671	C_8	215.2
γ	0.00993	C_9	143.1
r_c	8.32	C_{10}	4813.9

Table 6.1: Numerical values of the parameters of the Silvera-Goldman potential [65]. The values are given in atomic units (a.u.).

6.2 Normal Coordinates

For the RPMD method, the Hamiltonian can be written as

$$\mathcal{H}_P(\mathbf{p},\mathbf{q}) = \sum_{i=1}^{N}\sum_{k=1}^{P}\left(\frac{\left[p_i^{(k)}\right]^2}{2m} + \frac{1}{2}m\omega_P^2\left[q_i^{(k)} - q_i^{(k+1)}\right]^2\right) + \sum_{k=1}^{P} V_P\left(q_1^{(k)},\ldots,q_P^{(k)}\right), \quad (6.3)$$

where we had $\omega_P = (\beta_P\hbar)^{-1}$ and periodic indices, i.e. $P+1 \equiv 1$. Although this representation can technically be used to integrate the equations of motion without any problem, the implementation is awkward since the evolution equations are coupled due to the stiff springs connecting neighboring beads. The resulting harmonic forces are responsible for the occurring of many different time scales, which requires the use of very small time steps in order to obtain accurate results. This, of course, goes along with a significant increase in the computational cost.

While this problem is addressed in PIMC by only moving segments of the ring polymers at a time, this cannot be done in molecular dynamics simulations, since all particles need to be moved according to the acting forces at each time step. A possible solution is found in the fact that it is advantageous to split the Hamiltonian into two parts and consider the first sum in a different, more suitable representation. In fact, the first sum can be interpreted as a Hamiltonian with a harmonic potential. It is well-known that this system can be decoupled using so-called normal modes. Their use in RPMD has first been proposed by Tuckerman [71] as well as by Cao & Voth [11]. To derive this representation, we start by writing down the equations of motion as

$$\ddot{q}_i^{(j)} = -\omega_P^2\left(2q_i^{(j)} - q_i^{(j-1)} - q_i^{(j+1)}\right), \qquad 1 \le i \le N,\ 1 \le j \le P, \quad (6.4)$$

or, in matrix form,

$$\begin{pmatrix} \ddot{q}_i^{(1)} \\ \vdots \\ \vdots \\ \vdots \\ \ddot{q}_i^{(P)} \end{pmatrix} = -\omega_P^2 \begin{pmatrix} 2 & -1 & 0 & \cdots & 0 & -1 \\ -1 & 2 & -1 & 0 & \cdots & 0 \\ 0 & -1 & 2 & -1 & \cdots & 0 \\ \vdots & & & \ddots & & \vdots \\ 0 & \cdots & 0 & -1 & 2 & -1 \\ -1 & 0 & \cdots & 0 & -1 & 2 \end{pmatrix} \begin{pmatrix} q_i^{(1)} \\ \vdots \\ \vdots \\ \vdots \\ q_i^{(P)} \end{pmatrix}. \quad (6.5)$$

We immediately see that the involved matrix on the right hand side is real and symmetric. It is well known from linear algebra that a matrix $\mathbf{A}$ of this type can be diagonalized using its eigenvalues ω_k^2 and an orthogonal matrix $\mathbf{C}$ formed by the eigenvectors,

$$\mathbf{A} = \mathbf{C} \begin{pmatrix} \omega_{k_1}^2 & & \\ & \ddots & \\ & & \omega_{k_P}^2 \end{pmatrix} \mathbf{C}^T. \tag{6.6}$$

Note that we have already included the prefactor ω_P^2 from equation (6.5) into this representation. Inserting this into equation (6.5) and multiplying with $\mathbf{C}^T$ from the left, we obtain

$$\mathbf{C}^T \ddot{\mathbf{q}}_i = -\mathbf{C}^T \mathbf{C} \begin{pmatrix} \omega_{k_1}^2 & & \\ & \ddots & \\ & & \omega_{k_P}^2 \end{pmatrix} \mathbf{C}^T \mathbf{q}_i = - \begin{pmatrix} \omega_{k_1}^2 & & \\ & \ddots & \\ & & \omega_{k_P}^2 \end{pmatrix} \mathbf{C}^T \mathbf{q}_i. \tag{6.7}$$

At the price of considering transformed coordinates $\widehat{\mathbf{q}} := \mathbf{C}^T \mathbf{q}$, we have therefore decoupled the system of equations, such that we can integrate the equations of motion indepently for each normal mode. This is a huge advantage when it comes to the implementation and its related numerical difficulties. In particular, the problem of different time scales is remedied greatly. The corresponding transformation of the momenta is achieved similarly, yielding

$$\widehat{\mathbf{p}} = \mathbf{C} \cdot \mathbf{p}, \qquad \mathbf{p} = \mathbf{C}^T \cdot \widehat{\mathbf{p}}, \tag{6.8a}$$

$$\widehat{\mathbf{q}} = \mathbf{C} \cdot \mathbf{q}, \qquad \mathbf{q} = \mathbf{C}^T \cdot \widehat{\mathbf{q}}, \tag{6.8b}$$

where we also provided the formula for the inverse transformation. These transformed coordinates are called *normal coordinates* or *normal mode variables*, whereas the ω_k are called *normal mode frequencies.*

Remark

Note that $\mathbf{p}$ *and* $\mathbf{q}$ *as well as the corresponding normal mode coordinates comprise the beads of all* N *molecules, and is therefore a* $P \times N$ *matrix. All multiplications with* $\mathbf{C}$ *and* $\mathbf{C}^T$ *are therefore simple matrix multiplications.*

It now remains to calculate the eigenvalues and eigenvectors of $\mathbf{A}$ for our specific case. For an even number of beads, one possible orthogonal transformation matrix $\mathbf{C}$ is given by

$$C_{jk} = \begin{cases} \sqrt{1/P} & k = 1, \\ \sqrt{2/P} \cdot \cos\left[2j(k-1)\pi/P\right] & k = 2, \ldots, P/2 - 1, \\ \sqrt{1/P} \cdot (-1)^j & k = P/2, \\ \sqrt{2/P} \cdot \sin\left[2j(k-1)\pi/P\right] & k = P/2 + 1, \ldots, P, \end{cases} \tag{6.9}$$

while the normal frequencies ω_k are given by

$$\omega_k = 2\omega_P \sin\left(\frac{(k-1)\pi}{P}\right). \tag{6.10}$$

Note that the frequency corresponding to $k = 1$ is zero. The related normal mode coordinates therefore describe the movement of the center of mass of the molecule. It is furthermore of interest that in the case of a closed ring polymer, all eigenfrequencies except ω_1 appear twice, yielding only $P/2$ different frequencies. This will be important later on.

Neglecting the intermolecular potential, the Hamiltonian in the normal mode representation is then given by

$$\mathcal{H}^0(\widehat{\mathbf{p}}, \widehat{\mathbf{q}}) = \sum_{i=1}^{N} \sum_{k=1}^{P} \left(\frac{\left[\widehat{p}_i^{(k)}\right]^2}{2m} + \frac{1}{2} m \omega_k^2 \left[\widehat{q}_i^{(k)}\right]^2 \right). \tag{6.11}$$

It is even possible to exactly evolve the transformed system in time by updating the normal coordinates via

$$\left.\begin{pmatrix} \widehat{p}_i^{(k)} \\ \widehat{q}_i^{(k)} \end{pmatrix}\right|_{t+\Delta t} = \begin{pmatrix} \cos(\omega_k \Delta t) & -m\omega_k \sin(\omega_k \Delta t) \\ \sin(\omega_k \Delta t)/(m\omega_k) & \cos(\omega_k \Delta t) \end{pmatrix} \left.\begin{pmatrix} \widehat{p}_i^{(k)} \\ \widehat{q}_i^{(k)} \end{pmatrix}\right|_t. \tag{6.12}$$

6.3 The Algorithm

We have now set the basis to present the full algorithm used for the RPMD simulation together with a white noise Langevin thermostat, which is based on the description in [17]. The corresponding symmetric operator propagator is of the type

$$\mathrm{e}^{-\Delta t L} \approx \mathrm{e}^{-\frac{\Delta t}{2} L_\gamma} \mathrm{e}^{-\frac{\Delta t}{2} L_U} \mathrm{e}^{-\Delta t L_0} \mathrm{e}^{-\frac{\Delta t}{2} L_U} \mathrm{e}^{-\frac{\Delta t}{2} L_\gamma}, \tag{6.13}$$

where $L = L_0 + L_U + L_\gamma$ is the associated total Liouvillian. The particular procedure is described in Figure 6.2, where the five partitions marked by the dashed separation lines represent the decomposition of the total Liouvillian. Since there is a frequent change between bead and normal coordinates, we also present a graphical overview for one timestep focusing on those transformations in Figure 6.3.

Let us have a closer look at the respective steps and the quantities involved. The first part performs a half step under the Langevin term, which introduces the randomness due to the heat bath coupling to our system. This step is performed in the normal coordinate representation for simplicity of computation as well as exactness. The quantities $c_1^{(k)}$ and $c_2^{(k)}$ are given by

$$c_1^{(k)} = \mathrm{e}^{-\gamma^{(k)}\Delta t/2}, \qquad c_2^{(k)} = \sqrt{1-(c_1^{(k)})^2}, \tag{6.14}$$

while $\xi_i^{(k)}$ denotes a random variable drawn from a $\mathcal{N}(0,1)$ distribution. The $\gamma(k)$ denote the coupling strengths of the thermostats to the beads. We are free to choose their numerical values at our convenience, where the choice influences the speed of the exploration of the different energy shells.

In [17], it is argued that the optimal choice is $\gamma^{(k)} = 2\omega_k$. Note that steps 1 and 3 perform the change from bead to normal coordinate representation and back. Therefore, $\gamma^{(0)}$ represents the coupling strength of a thermostat to the center of mass, which should be handled differently than the other eigenmodes. To do so, we define a separate time constant τ_0, and choose

$$\gamma^{(0)} = \frac{1}{\tau_0}. \tag{6.15}$$

In Chapter 7, we will try different values for that parameter to investigate the effects on the system.

Parts 2 to 4 represent a standard velocity-Verlet step. It is important to note that step 6 performs the motion of the center of mass, while step 7 represents the evolution of the monomers under the free Hamiltonian (i.e. without intermolecular potentials and without thermostats). Both steps are performed in the normal coordinate representation as discussed in the previous section.

The last part then represents the second half of the "Langevin step", which is similar to part 1. Note that the set of random variables is freshly drawn for this step.

Langevin RPMD Algorithm

1. $\widehat{\mathbf{p}} \leftarrow \boldsymbol{C}^T \mathbf{p}$
2. $\widehat{p}_i^{(k)} \leftarrow c_1^{(k)} \widehat{p}_i^{(k)} + \sqrt{\frac{m_i}{\beta_n}} c_2^{(k)} \xi_i^{(k)}$
3. $\mathbf{p} \leftarrow \boldsymbol{C} \widehat{\mathbf{p}}$

---

4. $p_i^{(k)} \leftarrow p_i^{(k)} - \frac{\Delta t}{2} \frac{\partial V(q_1^{(k)}, \ldots, q_N^{(k)})}{\partial q_i^{(k)}}$

---

5. $\widehat{\mathbf{p}} \leftarrow \boldsymbol{C}^T \mathbf{p}$
   $\widehat{\mathbf{q}} \leftarrow \boldsymbol{C}^T \mathbf{q}$
6. $\begin{pmatrix} \widehat{p}_i^{(1)} \\ \widehat{q}_i^{(1)} \end{pmatrix} \leftarrow \begin{pmatrix} 1 & 0 \\ \Delta t/m & 1 \end{pmatrix} \begin{pmatrix} \widehat{p}_i^{(1)} \\ \widehat{q}_i^{(1)} \end{pmatrix}$
7. $\begin{pmatrix} \widehat{p}_i^{(k)} \\ \widehat{q}_i^{(k)} \end{pmatrix} \leftarrow \begin{pmatrix} \cos(\omega_k \Delta t) & -m\omega_k \sin(\omega_k \Delta t) \\ \sin(\omega_k \Delta t)/(m\omega_k) & \cos(\omega_k \Delta t) \end{pmatrix} \begin{pmatrix} \widehat{p}_i^{(k)} \\ \widehat{q}_i^{(k)} \end{pmatrix}$
8. $\mathbf{p} \leftarrow \boldsymbol{C} \widehat{\mathbf{p}}$
   $\mathbf{q} \leftarrow \boldsymbol{C} \widehat{\mathbf{q}}$

---

9. $p_i^{(k)} \leftarrow p_i^{(k)} - \frac{\Delta t}{2} \frac{\partial V(q_1^{(k)}, \ldots, q_N^{(k)})}{\partial q_i^{(k)}}$

---

10. $\widehat{\mathbf{p}} \leftarrow \boldsymbol{C}^T \mathbf{p}$
11. $\widehat{p}_i^{(k)} \leftarrow c_1^{(k)} \widehat{p}_i^{(k)} + \sqrt{\frac{m_i}{\beta_n}} c_2^{(k)} \xi_i^{(k)}$
12. $\mathbf{p} \leftarrow \boldsymbol{C} \widehat{\mathbf{p}}$

Figure 6.2: The algorithm for the RPMD simulation employing a Langevin thermostat.

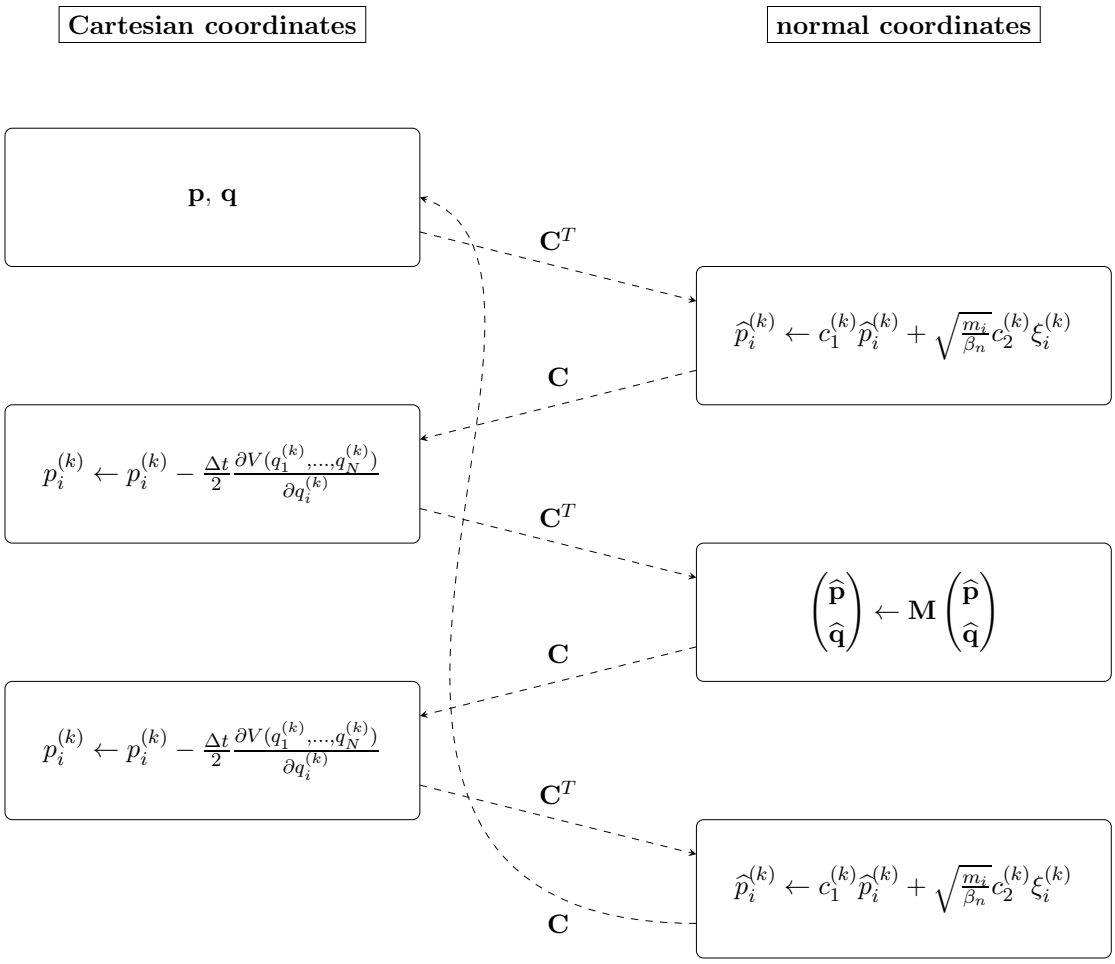

Figure 6.3: Graphical representation of the algorithm for white noise Langevin simulations. The manipulations in the left column are performed in Cartesian coordinates, the ones in the right column in normal coordinates. Note that the matrix multiplication in the fourth step represents steps 6 (the motion of the center of mass) and 7 (the motion of the monomers) in the algorithm.

6.4 Computational Parameters Used

In this section, we will briefly discuss the computational parameters we used in our simulations.

For each simulation, the procedure was as follows. After setting up the lattice, the system was evolved for 12.5 ps to obtain equilibrium. Then, the system was followed for 2.5 ns to record data. We always used 108 atoms and investigated different Trotter numbers ranging between 16 and 64. If nothing is indicated, we used P=64. With these parameters, one run took about 40 hours on a standard personal computer.

When considering macroscopic quantities in molecular dynamics simulations, there is a correlation between successive time steps, as has already been discussed in Chapter 3. Therefore, we need not analyze after every single step, but let the system evolve for some time and only calculate the macroscopic quantities every so often. Specifically, we sampled every ten evolution steps.

Next, for the calculation of the frequency spectra, it is important to choose the time stepsize as well as the recorded time-correlation length carefully in order to suppress noisy data. Here, we chose a time stepsize of $\Delta t = 2.5 \cdot 10^{-4}$ ps, and a maximum correlation length of $n_{\mathrm{cor}} = 50000$, corresponding to 12.5 ps. With this, the obtained spectra behaved nicely up to the calculated frequencies.

Chapter 7

Results

After all these preparations we can now turn to the presentation and discussion of the simulation results. The system we are investigating is liquid ortho-deuterium at temperatures in the range between 20 K and 37.5 K at densities for which the system is along the vapor-liquid coexistence line. What we will be actually interested in is the the velocity auto-correlation function (VACF), and, more importantly, its spectrum.

We start our investigation with RPMD simulations using Gaussian thermostats. The results of several simulations, i.e. those shown in Figure 7.1, have already been performed at the beginning of the particular investigation of this thesis and been provided in a private communication [51]. Obviously, they showed resonances in the spectrum of the VACF. Section 7.2 is therefore concerned with the investigation of the origin of those resonances, where also the dependence on temperature and Trotter number will be studied.

After this, we will turn to simulations using white-noise Langevin thermostats in Section 7.3. We will compare the respective results to data stemming not only from the RPMD simulations using Gaussian thermostats, but also from simulations using the CMD method. This will give interesting insights into the specificities of the different methods.

7.1 Ortho-Deuterium

In this work, we simulated the behavior of ortho-deuterium (o-D_2). The *ortho* configuration means that the nuclear spins are parallel oriented, which, at the investigated temperatures, is the case for almost 98% of the deuterium molecules [39].

Ortho-deuterium is – like para-hydrogen – in the rotational ground state for low temperatures, which is well described as forming of spherical particles [65]. If we considered the para-deuterium configuration, we would need to use an extended PIMC algorithm to take the rotatory wavefunction into account, which leads to much more complicated computations. Investigating the ortho-configuration, we do not need to worry about the orientation of the D–D bond, leading to a suitable description of the intermolecular potential by only taking radially symmetric pair interactions into account.

This simple geometry, together with the availability of experimental data, are the reasons D_2 has been used widely for studies addressing computational aspects in quantum mechanical systems [35, 57, 58]. Furthermore, many investigations on the system itself have been performed [15, 38, 48, 54] to compare the computational experiments to experimental data.

7.2 Calculations Using Gaussian Thermostats

We will start out with the discussion of the data obtained from the use of a Gaussian thermostat, which did not yield satisfactory results. Here, we will write $J(\omega) := C_{vv}^K(\omega)$ for the Kubo-transformed spectra, which will be the type of spectrum shown throughout this chapter. For the calculation of the spectrum we also used a Welch window with a cut-off of 5 ps.

We start out by considering VACF spectra of ortho-deuterium at different temperatures, where $N = 256$ and $P = 64$. They are shown in Figure 7.1. Note that the spectrum is shown in such a way that the diffusion constant D can be read off at $\omega = 0$. This is obtained based on the relation

$$D = \frac{1}{6} \int_{-\infty}^{\infty} \mathrm{d}t \, C_{vv}(t) = \frac{1}{6} J(0), \tag{7.1}$$

which will be the normalization kept throughout this chapter.

The qualitative difference of the respective graphs in Figure 7.1 is significant. It can be easily seen that the diffusion constant increases with increasing temperature. For comparison, the

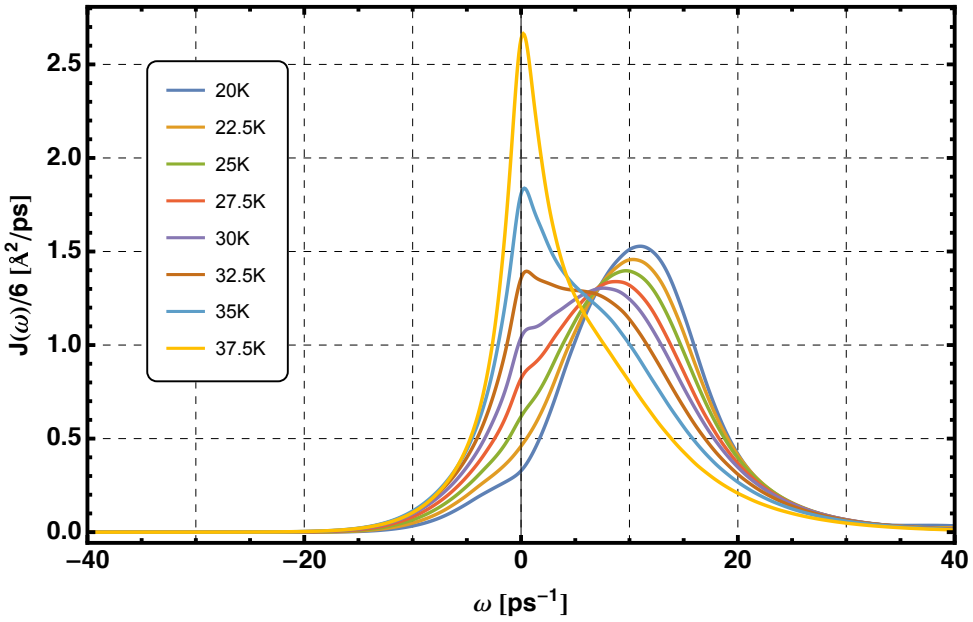

Figure 7.1: VACF Kubo-transformed spectra for D_2 obtained from RPMD simulations using Gaussian thermostats. The diffusion constant can be read off at $\omega = 0$.

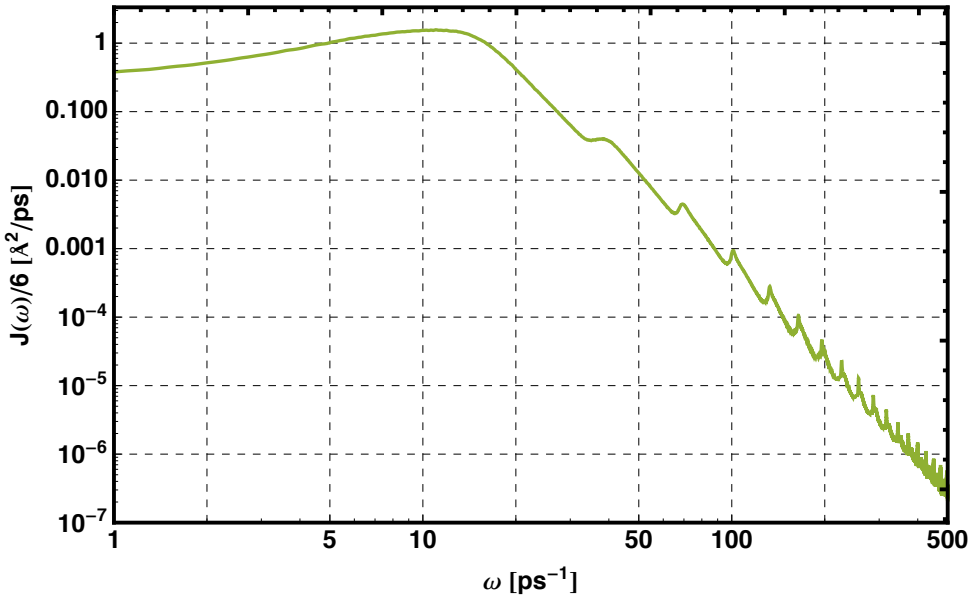

Figure 7.2: The VACF Kubo-transformed spectrum of D_2 calculated with a RPMD simulation using Gaussian thermostats at 20 K. The resonances at higher frequencies are clearly seen.

simulation at 20 K gives $D = 0.295\,\text{Å}^2\,\text{ps}^{-1}$, which is close to experimentally obtained data, $D = 0.36\,\text{Å}^2\,\text{ps}^{-1}$ [50].

However, we are interested in another observation. In Figure 7.2, the high-frequency range of the VACF spectrum for ortho-deuterium at 20 K, calculated from a RPMD simulation, is shown on a log-log scale. Here, we used $N = 108$ and $P = 64$. Note that we actually have $N + 1$ thermostats, since each ring polymer is attached to its individual thermostat keeping its "internal" temperature at $P \cdot T$, and one additional, global, thermostat keeping the whole system at temperature T.

As can be seen, there are several resonances at larger frequencies. Although it is emphasized that these resonances are very small and probably won't affect the numerical values obtained by integration over the whole spectrum, there is still the question of their origin.

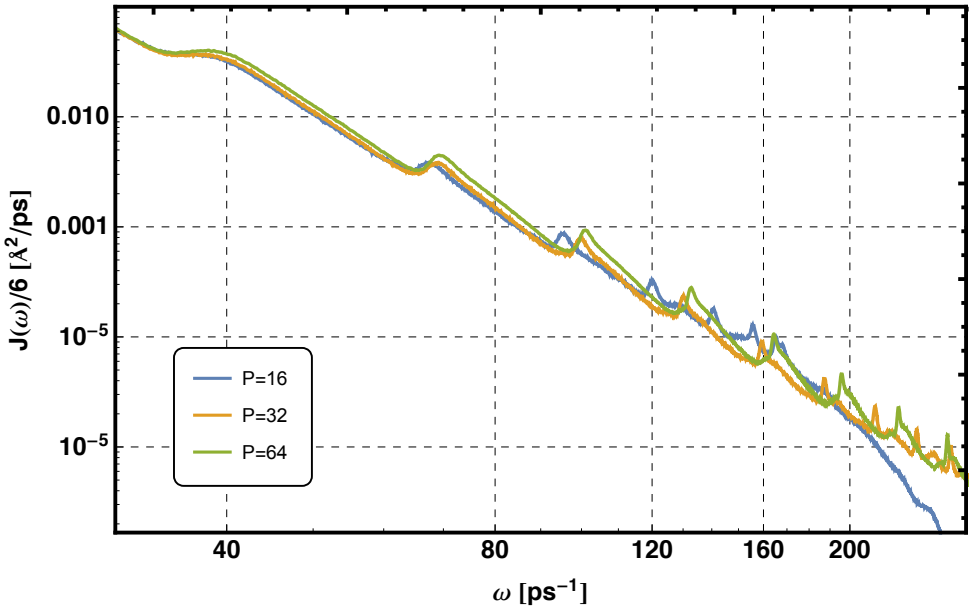

Figure 7.3: Part of the VACF spectrum of D_2 at 20 K calculated with a RPMD simulation employing Gaussian thermostats for different Trotter numbers. The dependence on P is obvious. Note that only a part of the spectrum is shown for a better comparison of the resonance locations.

To gain insight on this question, we considered spectra for Trotter numbers $P = 16$, $P = 32$, and $P = 64$, and for several temperatures T between 20 K and 37.5 K. Note that the simulations for different temperatures have all been performed at the vapor-liquid coexistence

temperature T [K]	density ρ [nm^{-3}]
20	25.60
22.5	24.75
25	23.84
27.5	22.65
30	21.53
32.5	19.93
35	17.93
37.5	14.69

Table 7.1: Temperatures and number densities that have been used for the simulations of ortho-deuterium. Values taken from [62].

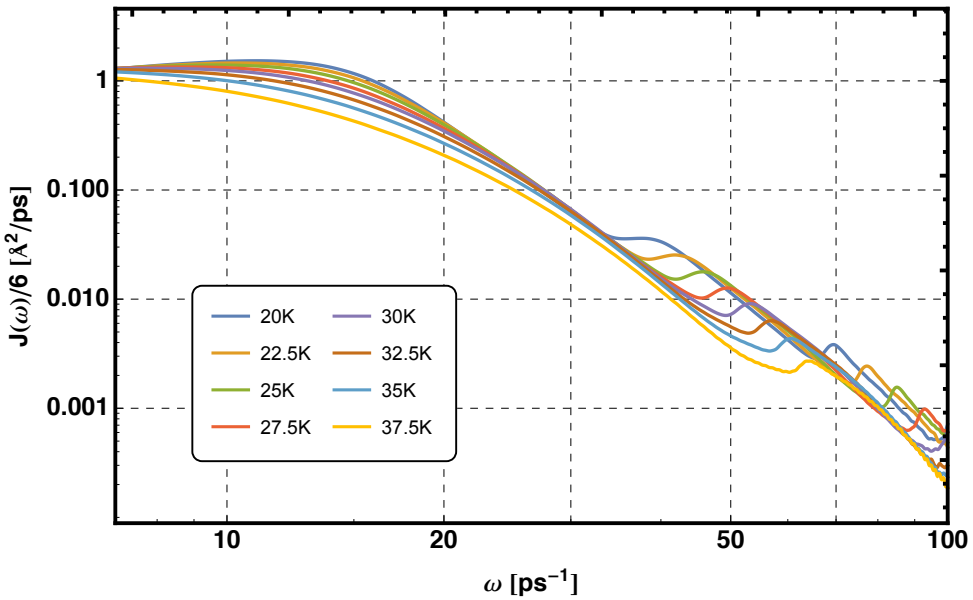

Figure 7.4: The VACF spectrum of D_2 calculated with a RPMD simulation employing Gaussian thermostats for different temperatures. The dependence on T is obvious. In these simulations, the Trotter number was kept constant at $P = 64$.

curve, which is the reason why different densities were used. The input parameters for T and ρ are shown in Table 7.1. The results are shown in Figures 7.3 and 7.4. It is obvious that the resonance positions depend on both of these parameters.

Having found those two dependencies, we should now try to find an explicit relationship between those quantities. We start with the following, qualitative, observation: On the one hand, the overall number of resonances turns out to be the same as the half the Trotter number. This fact has been observed in the spectrum using $P = 16$, where the resonances are all below $\omega = 200\,\mathrm{ps}^{-1}$. On the other hand, every eigenfrequency in the ring polymer appears twice due to the periodicity condition for a closed ring polymer, yielding half as many eigenfrequencies as beads. This has already been discussed in Section 6.2. That correspondence is a first clue regarding the origin of those resonances.

The next step is therefore a comparison of the resonance frequencies to the eigenfrequencies of the ring polymers, which depend on both P and T. This comparison for $P = 64$ at $20\,\mathrm{K}$ is presented in Figure 7.5. For better resolution, a detailed comparison at large frequencies is shown in Figure 7.6. We see that the correspondence is obvious, although there is no exact agreement between the two. Rather, for low frequencies, the eigenfrequencies are lower than the observed resonances, whereas it is the other way round for high frequencies. A possible explanation for this deviation is that the resonance frequencies in the simulation are also affected by the intermolecular potential. This interaction then leads to a small shift of the resonances compared to a free ring polymer.

Nevertheless, these findings prove that those resonances are induced by the eigenmodes of the ring polymer. While observing such resonances for a classical ring polymer would definitely make sense as this is an inherent effect, this is not true for the path integral approach. Here, the ring polymer is a purely fictitious device and only appears due to the imaginary time path integral formulation, and therefore those resonances do not represent any physical process in the system. As a consequence, this effect is unwanted and should be avoided. To this end, we turn to a Langevin thermostat and investigate the velocity auto-correlation spectrum for this approach.

7.3 Calculations Using a White-Noise Langevin Thermostat

For this type of simulations, we use the algorithm described in Figure 6.2. Note that the Langevin approach employs one independent thermostat per monomer, thereby using $P \cdot N$ thermostats in general, while the Gaussian approach only uses $N + 1$ thermostats. As has been discussed during the presentation of the approach in Chapter 6, when using a white-noise Langevin thermostat, there is one parameter left for adjustment. This is the coupling

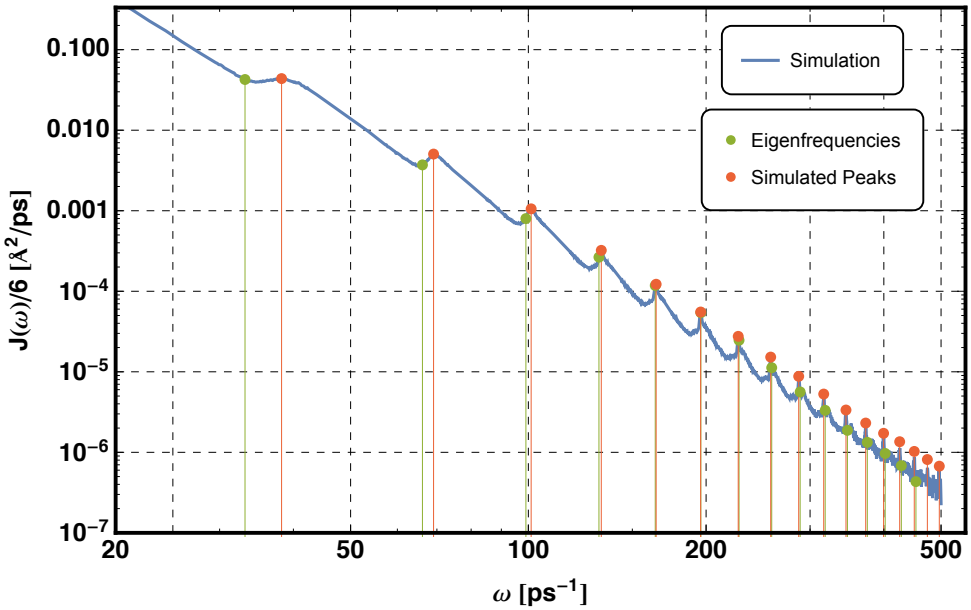

Figure 7.5: Comparison of the resonances in the VACF spectrum of D_2 to the polymers' eigenfrequencies for $P = 64$ at 20 K. The qualitative correspondence is clear. For low ω, the eigenfrequencies are lower than the resonances, while it is the other way round for high ω.

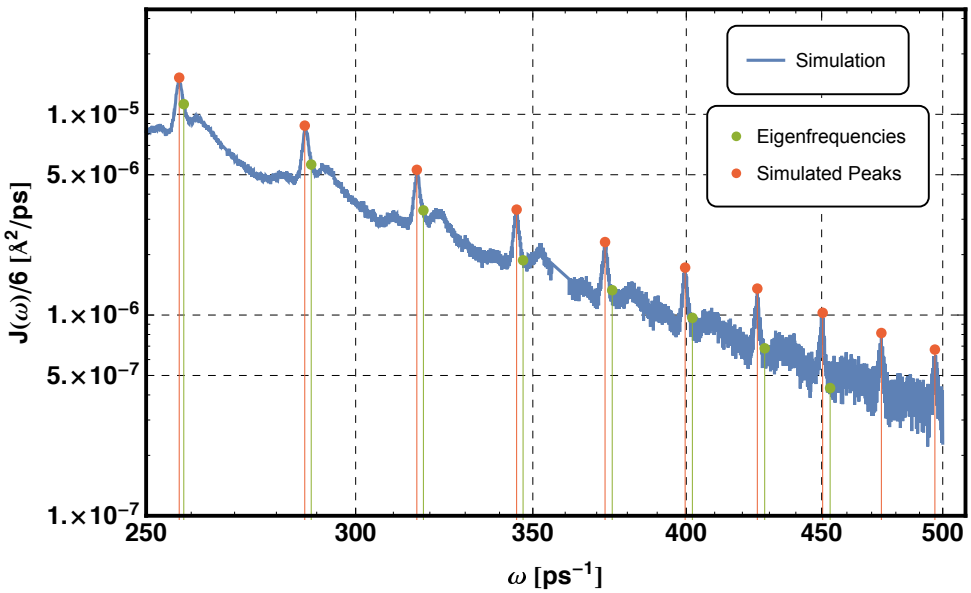

Figure 7.6: Zoom into the high frequencies from Figure 7.5. In this region, the eigenfrequencies are larger than the resonance frequencies.

strength of the stochastic collisions to the system, which is given by the parameter τ_0. We therefore calculated the spectra at 20 K employing different numerical values for τ_0. Figure 7.7 shows the spectra for τ_0 equal to 1, 10, and ∞.

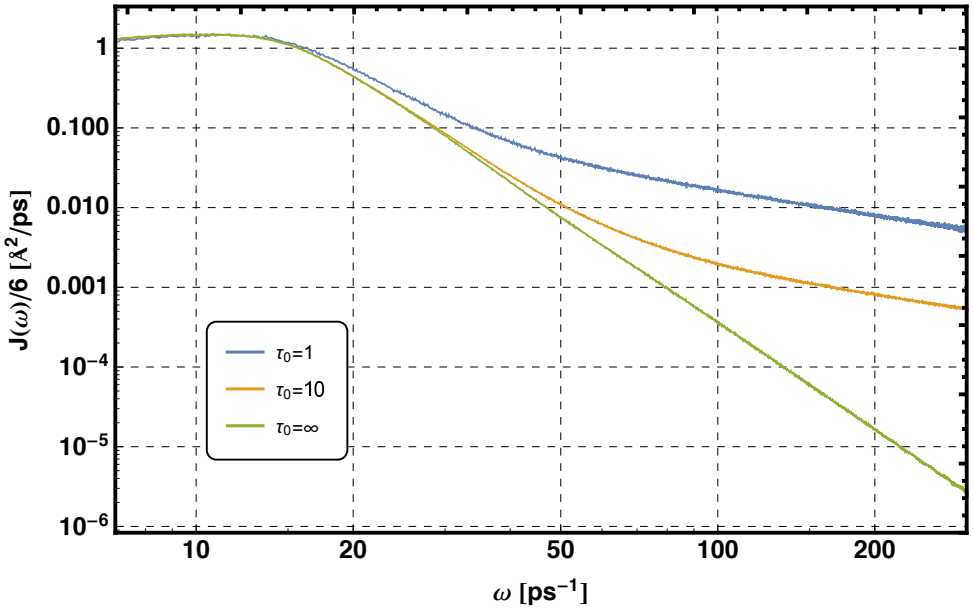

Figure 7.7: VACF spectrum of D_2 at 20 K calculated using RPMD and Langevin thermostats with different coupling strengths.

Obviously, in all cases, the spectrum remains free of resonances. However, the decrease at high frequencies differs greatly for larger values of τ_0. This means that for larger τ_0, the contributions of the high frequencies become more and more suppressed. This poses the question regarding the correct suppression strength induced by τ_0. Since it has been mentioned in the literature that there should not be a thermostat attached to the polymers' center of mass [17], which corresponds to setting $\tau_0 = \infty$, this choice appears to be suitable. A comparison of this setup to the results obtained from the Gaussian thermostat shows that this is indeed the correct choice (see Figure 7.8).

For the spectra obtained from the RPMD simulations with Gaussian thermostats and from the Langevin algorithm with $\tau_0 = \infty$, it is also interesting to compare the velocity auto-correlation function itself, which is shown in Figure 7.9. Here, we also included the results stemming from a simulation employing the CMD method [51], which employed one global Gaussian thermostat. All three functions agree for almost all t, apart from an obvious difference in the

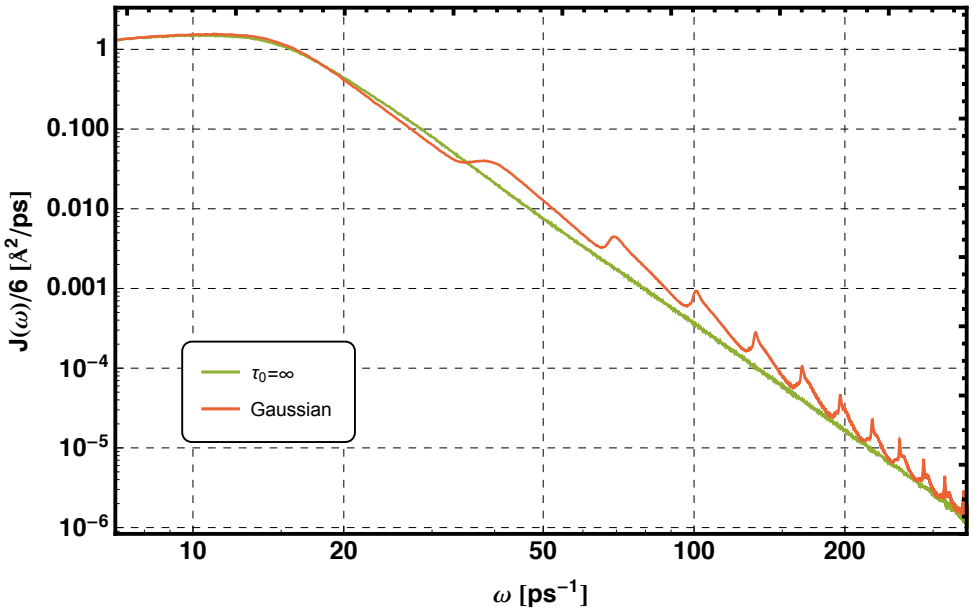

Figure 7.8: Comparison of the VACF spectrum of D_2 obtained by RPMD using Gaussian thermostats and Langevin thermostats with $\tau_0 = \infty$ at 20 K.

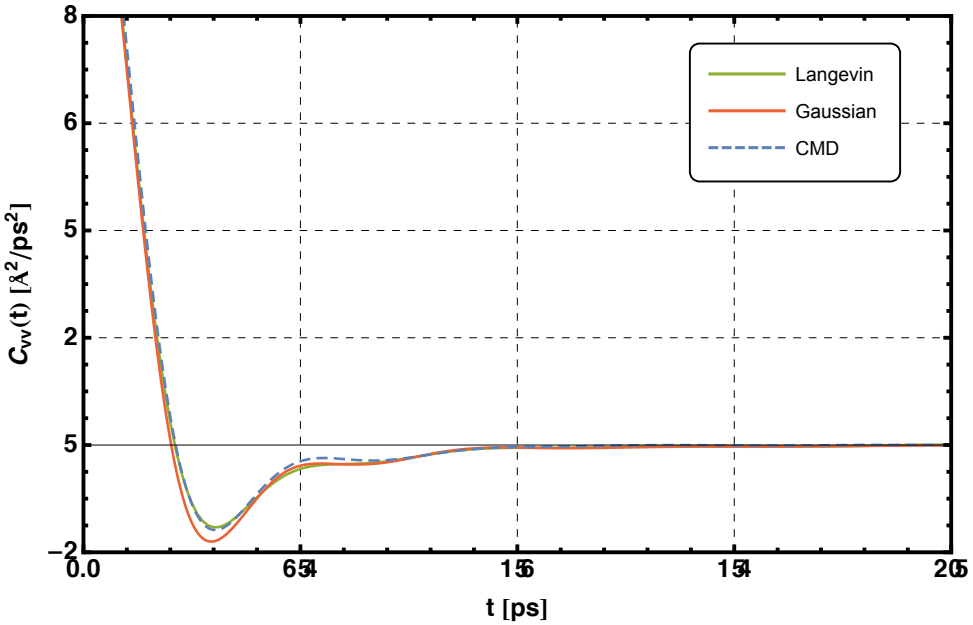

Figure 7.9: Comparison of the velocity auto-correlation functions for D_2 at 20 K using RPMD simulations with Gaussian thermostats, Langevin thermostats with $\tau_0 = \infty$, and the CMD method.

region of the minimum around $t = 0.3\,\mathrm{ps}$. There, the auto-correlation function of the RPMD simulation with Gaussian thermostats differs from the other two. It is worth noting that the Langevin system shows excellent agreement with the VACF computed with the CMD method.

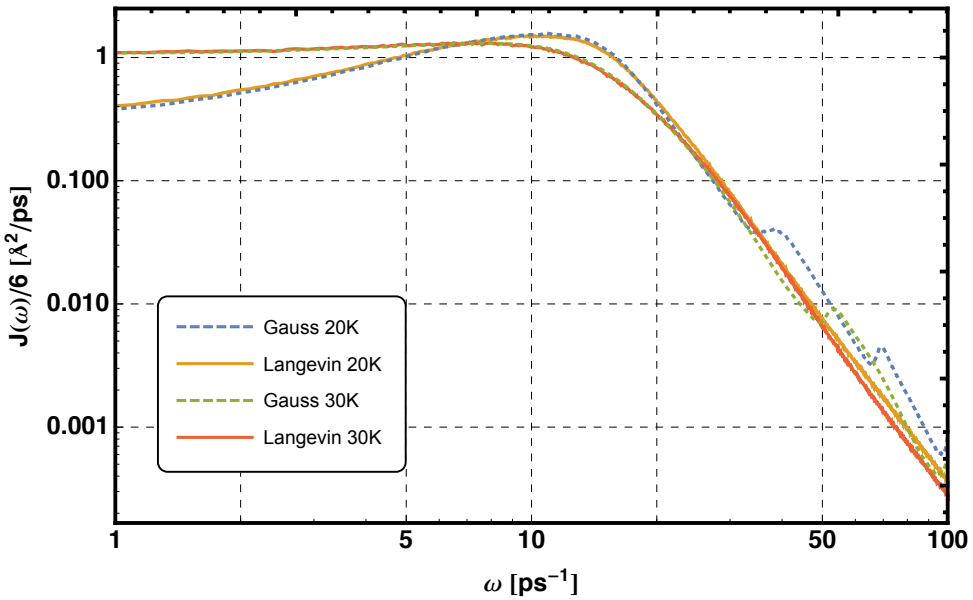

Figure 7.10: Comparison of the Gauss and the Langevin VACF spectra for D_2 at 20 K and 30 K. The agreement for different temperatures at high frequencies could not be inferred from the Gauss spectra.

Finally, we are interested in the spectra calculated using Langevin thermostats at different temperatures. In particular, we present the respective curves for $T = 20\,\mathrm{K}$ and $T = 30\,\mathrm{K}$. We show the corresponding results together with a comparison to the data from the simulations employing Gaussian thermostats in Figure 7.10. The general agreement, apart from the resonances in the Gauss spectra, is obvious.

Furthermore, looking only at the Langevin curves, it is observed that while the spectra show a considerable difference at low frequencies for different temperatures, the high frequencies are almost unaffected by a temperature change. This behavior could not be discerned in the RPMD simulations employing Gaussian thermostats due to the resonances, which lead to artifacts in the curves.

Based on this finding one might be tempted to wonder if this behavior, i.e. the agreement at high frequencies, is also seen in CMD simulations. The spectra in question are shown in Figure 7.11. There are several conclusions to be drawn. First, the CMD spectra show

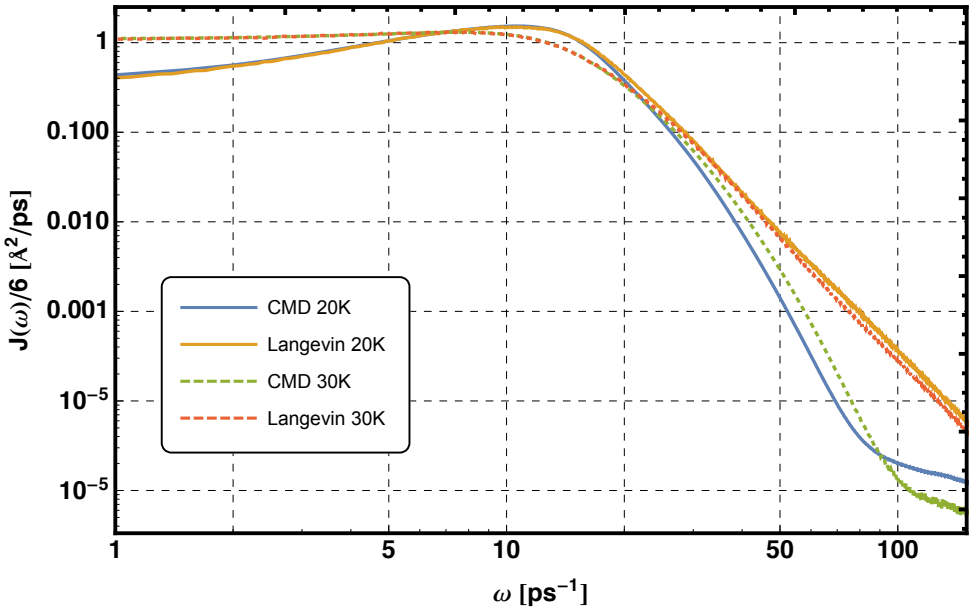

Figure 7.11: Comparison of RPMD using Langevin thermostats to the VACF spectrum for D_2 obtained from the CMD method at 20 K and 30 K.

much lower values in the high-frequency region compared to the Langevin spectra. Second, the CMD curves do not show the same agreement as the one seen in the Langevin spectra. Finally, there is a characteristic knee in the spectra around 100 ps^{-1}, whose position obviously depends on the temperature, too. However, this might also be an artifact, but this question is not in the scope of this thesis. These differences are based on the diverse approximations induced by the derivation of CMD and RPMD methods.

7.4 Conclusions

A closer investigation of the resonances in the VACF spectra in the simulations using Gaussian thermostats showed the correspondence to the eigenfrequencies of the ring polymers. This turned out to be problematic, since those eigenfrequencies are only a virtual construct to be able to perform a classical-like molecular dynamics simulation, and therefore do not correspond to any physical process taking place in the system under investigation. Furthermore, those resonances prevent a comparison of the spectra at high frequencies.

By using a Langevin thermostat, we were able to eliminate those resonances. We also showed the different results for different coupling strengths, and argued the choice of not coupling a

thermostat to the normal mode corresponding to the center of mass. The comparison of the high frequencies of the spectra for different temperatures showed that the curves are almost independent of T in this region. This poses the question if this is just a coincidence of a general result for this system.

A comparison to the CMD method showed good agreement of the VACF itself, but revealed differences – although only in the high-frequency region – in the spectra.

Chapter 8

Conclusions

In this work, we investigated the calculation of the spectrum of the velocity auto-correlation function in quantum mechanical systems. To this end, we used ring polymer molecular dynamics simulations, where Feynman's path integral formalism was employed. These methods, although just leading to an approximation of the velocity auto-correlation function, proves to be a very convenient and, for moderately quantum mechanical systems, rather accurate tool.

For the proper implementation, we used several well-known techniques. As an example, we used a normal mode transformation for the ring polymer beads, which allows an exact propagation of the system under the free Hamiltonian. To couple the system with a heat bath, we employed two different types of thermostats.

The results presented in the previous chapter revealed the importance of a suitable thermostat. We have seen that when using Gaussian thermostats, the spectrum of the auto-correlation function shows resonances, which prevents a proper interpretation of the high-frequency region of the spectrum. We could identify these resonances as corresponding to the eigenfrequencies of the ring-polymer beads. This is especially problematic, since those eigenmodes represent a non-physical process in our system.

The use of Langevin thermostats, on the other hand, did not show such resonances. As a consequence, the method proved to be much more suitable for the calculation of the desired spectra. The investigation of different coupling strengths showed the great differences that can arise due to different choices for the numerical values, and which value should be chosen for the best results.

Based on this investigation, several further questions arise that might be of interest in subsequent studies. One the one hand, several new observations have been made. As an example, it might be of interest whether the independence from temperature in the high frequency region of the spectrum is just a coincidence or a general result for weakly quantum mechanical systems. On the other hand, the question is whether the observations made in these simulations can also be made using other, e.g. strongly quantum mechanical systems like H_2.

Bibliography

[1] Alder, B. and Wainwright, T. Molecular dynamics by electronic computers. *Transport Processes in Statistical Mechanics*, pages 97–131, 1958

[2] Allen, M.P. and Tildesley, D.J. *Computer simulation of liquids*. Oxford University Press, 1989

[3] Andersen, H.C. Molecular dynamics simulations at constant pressure and/or temperature. *The Journal of Chemical Physics*, **72**(4): 2384–2393, 1980

[4] Balucani, U. and Zoppi, M. Dynamics of the Liquid State. *Oxford, Oxford University Press*, **1**: 994, 1994

[5] Bernal, J.D. The Bakerian lecture, 1962. The structure of liquids. *Proceedings of the Royal Society of London. Series A, Mathematical and Physical Sciences*, **280**(1382): 299–322, 1964

[6] Boninsegni, M. and Ceperley, D.M. Path Integral Monte Carlo simulation of isotopic liquid helium mixtures. *Physical Review Letters*, **74**(12): 2288, 1995

[7] Born, M. and Von Karman, T. Über Schwingungen in Raumgittern. *Physikalische Zeitschrift*, **13**: 297–309, 1912

[8] Bussi, G. and Parrinello, M. Accurate sampling using Langevin dynamics. *Physical Review E*, **75**(5): 056707, 2007

[9] Cao, J. and Voth, G.A. A new perspective on quantum time correlation functions. *The Journal of Chemical Physics*, **99**(12): 10070–10073, 1993

[10] Cao, J. and Voth, G.A. The formulation of quantum statistical mechanics based on the Feynman path centroid density. I. Equilibrium properties. *The Journal of Chemical Physics*, **100**(7): 5093–5105, 1994

[11] Cao, J. and Voth, G.A. The formulation of quantum statistical mechanics based on the Feynman path centroid density. II. Dynamical properties. *The Journal of Chemical Physics*, **100**(7): 5106–5117, 1994

[12] Cao, J. and Voth, G.A. The formulation of quantum statistical mechanics based on the Feynman path centroid density. III. Phase space formalism and analysis of centroid molecular dynamics. *The Journal of Chemical Physics*, **101**(7): 6157–6167, 1994

[13] Cao, J. and Voth, G.A. The formulation of quantum statistical mechanics based on the Feynman path centroid density. IV. Algorithms for centroid molecular dynamics. *The Journal of Chemical Physics*, **101**(7): 6168–6183, 1994

[14] Car, R. and Parrinello, M. Unified approach for molecular dynamics and density-functional theory. *Physical Review Letters*, **55**(22): 2471, 1985

[15] Cazorla, C. and Boronat, J. Two-dimensional molecular para-hydrogen and ortho-deuterium at zero temperature. *Physical Review B*, **78**(13): 134509, 2008

[16] Ceperley, D.M. Path integrals in the theory of condensed helium. *Reviews of Modern Physics*, **67**(2): 279, 1995

[17] Ceriotti, M., Parrinello, M., Markland, T.E., and Manolopoulos, D.E. Efficient stochastic thermostatting of path integral molecular dynamics. *The Journal of Chemical Physics*, **133**(12): 124104, 2010

[18] Chandler, D. and Wolynes, P.G. Exploiting the isomorphism between quantum theory and classical statistical mechanics of polyatomic fluids. *The Journal of Chemical Physics*, **74**(7): 4078–4095, 1981

[19] Chen, B., Ivanov, I., Klein, M.L., and Parrinello, M. Hydrogen bonding in water. *Physical Review Letters*, **91**(21): 215503, 2003

[20] Craig, I.R. *Ring polymer molecular dynamics*. Ph.D. thesis, University of Oxford, 2006

[21] Craig, I.R. and Manolopoulos, D.E. Quantum statistics and classical mechanics: Real time correlation functions from ring polymer molecular dynamics. *The Journal of Chemical Physics*, **121**(8): 3368–3373, 2004

[22] Craig, I.R. and Manolopoulos, D.E. Chemical reaction rates from ring polymer molecular dynamics. *The Journal of Chemical Physics*, **122**(8): 084106, 2005

[23] Dang, L.X. and Chang, T.M. Molecular dynamics study of water clusters, liquid, and liquid–vapor interface of water with many-body potentials. *The Journal of Chemical Physics*, **106**(19): 8149–8159, 1997

[24] Daw, M.S. and Baskes, M.I. Embedded-atom method: Derivation and application to impurities, surfaces, and other defects in metals. *Physical Review B*, **29**(12): 6443, 1984

[25] Fermi, E., Pasta, J., and Ulam, S. Studies of nonlinear problems. *Los Alamos Report LA-1940*, **978**, 1955

[26] Feynman, R.P. Space-time approach to non-relativistic quantum mechanics. *Reviews of Modern Physics*, **20**(2): 367, 1948

[27] Frenkel, D. and Smit, B. *Understanding Molecular Simulation: From Algorithms to Applications*, volume 1. Elsevier (formerly published by Academic Press), 2002

[28] Guarini, E., Neumann, M., Bafile, U., Celli, M., Colognesi, D., Bellissima, S., Farhi, E., and Calzavara, Y. Velocity autocorrelation by quantum simulations for direct parameter-free computations of the neutron cross sections. II. Liquid deuterium. *Physical Review B*, **93**(22): 224302, 2016

[29] Guarini, E., Neumann, M., Bafile, U., Celli, M., Colognesi, D., Farhi, E., and Calzavara, Y. Velocity autocorrelation in liquid parahydrogen by quantum simulations for direct parameter-free computations of neutron cross sections. *Physical Review B*, **92**(10): 104303, 2015

[30] Habershon, S., Manolopoulos, D.E., Markland, T.E., and Miller III, T.F. Ring-polymer molecular dynamics: Quantum effects in chemical dynamics from classical trajectories in an extended phase space. *Annual Review of Physical Chemistry*, **64**: 387–413, 2013

[31] Habershon, S., Markland, T.E., and Manolopoulos, D.E. Competing quantum effects in the dynamics of a flexible water model. *The Journal of Chemical Physics*, **131**(2): 024501, 2009

[32] Hall, R.W. and Berne, B.J. Nonergodicity in path integral molecular dynamics. *The Journal of Chemical Physics*, **81**(8): 3641–3643, 1984

[33] Harp, G. and Berne, B.J. Linear-and Angular-Momentum Autocorrelation Functions in Diatomic Liquids. *The Journal of Chemical Physics*, **49**(3): 1249–1254, 1968

[34] Hone, T.D., Rossky, P.J., and Voth, G.A. A comparative study of imaginary time path integral based methods for quantum dynamics. *The Journal of Chemical Physics*, **124**(15): 154103, 2006

[35] Hone, T.D. and Voth, G.A. A centroid molecular dynamics study of liquid para-hydrogen and ortho-deuterium. *The Journal of Chemical Physics*, **121**(13): 6412–6422, 2004

[36] Hoover, W.G. Canonical dynamics: equilibrium phase-space distributions. *Physical Review A*, **31**(3): 1695, 1985

[37] Hoover, W.G. Constant-pressure equations of motion. *Physical Review A*, **34**(3): 2499, 1986

[38] Janssen, W. and Van der Avoird, A. Dynamics and phase transitions in solid ortho and para hydrogen and deuterium from an ab initio potential. *Physical Review B*, **42**(1): 838, 1990

[39] Johnston, H.L. and Long, E.A. Heat Capacity Curves of the Simpler Gases. VI. Rotational Heat Capacity Curves of Molecular Deuterium and of Deuterium Hydride. The Equilibrium Between the Ortho and Para Forms of Deuterium. Free Energy, Total Energy, Entropy, Heat Capacity and Dissociation of H^2H^2 and of H^1H^2, to 3000° K^1. *The Journal of Chemical Physics*, **2**(7): 389–395, 1934

[40] Kubo, R. Statistical-mechanical theory of irreversible processes. I. General theory and simple applications to magnetic and conduction problems. *Journal of the Physical Society of Japan*, **12**(6): 570–586, 1957

[41] Kumar, R. and Singh, S. Temperature Variation of Second Virial Coefficient and Viscosity for Deuterium (D_2). *International Archive of Applied Sciences and Technology*, **7**(1): 16–20, 2016

[42] Levitt, M. and Warshel, A. Computer simulation of protein folding. *Nature*, **253**(5494): 694–698, 1975

[43] Markland, T.E., Habershon, S., and Manolopoulos, D.E. Quantum diffusion of hydrogen and muonium atoms in liquid water and hexagonal ice. *The Journal of Chemical Physics*, **128**(19): 194506, 2008

[44] Markland, T.E., Morrone, J.A., Miyazaki, K., Berne, B.J., Reichman, D.R., and Rabani, E. Theory and simulations of quantum glass forming liquids. *The Journal of Chemical Physics*, **136**(7): 074511, 2012

[45] Martyna, G.J., Klein, M.L., and Tuckerman, M. Nosé–Hoover chains: the canonical ensemble via continuous dynamics. *The Journal of Chemical Physics*, **97**(4): 2635–2643, 1992

[46] McCammon, J.A., Gelin, B.R., and Karplus, M. Dynamics of folded proteins. *Nature*, **267**(5612): 585–590, 1977

[47] Metropolis, N., Rosenbluth, A.W., Rosenbluth, M.N., Teller, A.H., and Teller, E. Equation of state calculations by fast computing machines. *The Journal of Chemical Physics*, **21**(6): 1087–1092, 1953

[48] Miller III, T.F. and Manolopoulos, D.E. Quantum diffusion in liquid parahydrogen from ring-polymer molecular dynamics. *The Journal of Chemical Physics*, **122**(18): 184503, 2005

[49] Morriss, G.P. and Evans, D.J. *Statistical Mechanics of Nonequilbrium Liquids*. ANU Press, 2007

[50] Mukherjee, M., Bermejo, F., Fåk, B., and Bennington, S. Microscopic dynamics in liquid deuterium: A transition from collective to single-particle regimes. *EPL (Europhysics Letters)*, **40**(2): 153, 1997

[51] Neumann, M. private communication, 2016

[52] Nosé, S. A molecular dynamics method for simulations in the canonical ensemble. *Molecular Physics*, **52**(2): 255–268, 1984

[53] Nosé, S. A unified formulation of the constant temperature molecular dynamics methods. *The Journal of Chemical Physics*, **81**(1): 511–519, 1984

[54] Operetto, F. and Pederiva, F. Diffusion Monte Carlo study of the equation of state of solid ortho-D_2. *The Journal of Chemical Physics*, **126**(7): 074704–074704, 2007

[55] Parrinello, M. and Rahman, A. Study of an F center in molten KCl. *The Journal of Chemical Physics*, **80**(2): 860–867, 1984

[56] Pollock, E. and Ceperley, D. Simulation of quantum many-body systems by path-integral methods. *Physical Review B*, **30**(5): 2555, 1984

[57] Rabani, E. and Reichman, D. Collective and single-particle dynamics in liquid orthodeuterium: A quantum mode-coupling approach. *EPL (Europhysics Letters)*, **60**(5): 656, 2002

[58] Rabani, E. and Reichman, D.R. A fully self-consistent treatment of collective fluctuations in quantum liquids. *The Journal of Chemical Physics*, **120**(3): 1458–1465, 2004

[59] Rahman, A. Correlations in the motion of atoms in liquid argon. *Physical Review*, **136**(2A): A405, 1964

[60] Rahman, A., Singwi, K., and Sjölander, A. Theory of slow neutron scattering by liquids. I. *Physical Review*, **126**(3): 986, 1962

[61] Rahman, A. and Stillinger, F.H. Molecular dynamics study of liquid water. *The Journal of Chemical Physics*, **55**(7): 3336–3359, 1971

[62] Roder, H.M., Childs, G., McCarty, R., and Angerhofer, P. Survey of the properties of the hydrogen isotopes below their critical temperatures. Technical report, National Bureau of Standards, Boulder, Colorado (USA). Institute for Basic Standards, 1973

[63] Rossi, M., Ceriotti, M., and Manolopoulos, D.E. How to remove the spurious resonances from ring polymer molecular dynamics. *The Journal of Chemical Physics*, **140**(23): 234116, 2014

[64] Schulman, L.S. *Techniques and Applications of Path Integration.* J. Wiley and Sons, New York, 1981

[65] Silvera, I.F. and Goldman, V.V. The isotropic intermolecular potential for H_2 and D_2 in the solid and gas phases. *The Journal of Chemical Physics*, **69**(9): 4209–4213, 1978

[66] Stillinger, F.H. and Weber, T.A. Computer simulation of local order in condensed phases of silicon. *Physical Review B*, **31**(8): 5262, 1985

[67] Swope, W.C., Andersen, H.C., Berens, P.H., and Wilson, K.R. A computer simulation method for the calculation of equilibrium constants for the formation of physical clusters of molecules: Application to small water clusters. *The Journal of Chemical Physics*, **76**(1): 637–649, 1982

[68] Thirumalai, D., Hall, R.W., and Berne, B.J. A path integral Monte Carlo study of liquid neon and the quantum effective pair potential. *The Journal of Chemical Physics*, **81**(6): 2523–2527, 1984

[69] Tobias, D.J., Martyna, G.J., and Klein, M.L. Molecular dynamics simulations of a protein in the canonical ensemble. *The Journal of Physical Chemistry*, **97**(49): 12959–12966, 1993

[70] Tuckerman, M. *Statistical mechanics: theory and molecular simulation*. Oxford University Press, 2010

[71] Tuckerman, M.E., Berne, B.J., Martyna, G.J., and Klein, M.L. Efficient molecular dynamics and hybrid Monte Carlo algorithms for path integrals. *The Journal of Chemical Physics*, **99**(4): 2796–2808, 1993

[72] Verlet, L. Computer "experiments" on classical fluids. I. Thermodynamical properties of Lennard-Jones molecules. *Physical Review*, **159**(1): 98, 1967